© 2021. Published by The Company of Biologists Ltd | Journal of Cell Science (2021) 134, jcs258578. doi:10.1242/jcs.258578

RESEARCH ARTICLE

The oncogenic transcription factor FUS-CHOP can undergo nuclear liquid–liquid phase separation

Izzy Owen[1], Debra Yee[1], Hala Wyne[1], Theodora Myrto Perdikari[2], Victoria Johnson[3], Jeremy Smyth[4], Robert Kortum[5], Nicolas L. Fawzi[3] and Frank Shewmaker[1,*]

ABSTRACT

Myxoid liposarcoma is caused by a chromosomal translocation resulting in a fusion protein comprised of the N terminus of FUS (fused in sarcoma) and the full-length transcription factor CHOP (CCAAT/enhancer-binding protein homologous protein, also known as DDIT3). FUS functions in RNA metabolism, and CHOP is a stress-induced transcription factor. The FUS-CHOP fusion protein causes unique gene expression and oncogenic transformation. Although it is clear that the FUS segment is required for oncogenic transformation, the mechanism of FUS-CHOP-induced transcriptional activation is unknown. Recently, some transcription factors and super enhancers have been proposed to undergo liquid–liquid phase separation and form membraneless compartments that recruit transcription machinery to gene promoters. Since phase separation of FUS depends on its N terminus, transcriptional activation by FUS-CHOP could result from the N terminus driving nuclear phase transitions. Here, we characterized FUS-CHOP in cells and *in vitro*, and observed novel phase-separating properties relative to unmodified CHOP. Our data indicate that FUS-CHOP forms phase-separated condensates that colocalize with BRD4, a marker of super enhancer condensates. We provide evidence that the FUS-CHOP phase transition is a novel oncogenic mechanism and potential therapeutic target for myxoid liposarcoma.

This article has an associated First Person interview with the first author of the paper.

KEY WORDS: CHOP, FUS, Liquid–liquid phase separation, Oncogenic fusion protein, Transcriptional activation

INTRODUCTION

Soft tissue sarcomas (STSs) are diagnosed in roughly 12,000 patients in the United States each year, with a mortality rate of ∼40% (Siegel et al., 2015). Liposarcoma is the most common type of STS, accounting for ∼20% of all adult STS diagnoses (Bock et al., 2020; Perez-Losada et al., 2000). Myxoid liposarcoma (MLS) is the second most common liposarcoma and is distinguished by the cytogenetic hallmark of t(12;16)(q13;p11) (Bock et al., 2020; Suzuki et al., 2012). This chromosomal translocation creates a novel fusion protein composed of the N terminus of FUS (fused in sarcoma) and full-length CHOP (CCAAT/enhancer-binding protein homologous protein, also known as DDIT3).

FUS is a ubiquitously expressed, predominantly nuclear DNA- and RNA-binding protein that functions in the DNA damage response, transcription and RNA metabolism (Chen et al., 2019a; Tan et al., 2012; Zinszner et al., 1997). The N-terminal prion-like domain of FUS (PrLD; amino acids ∼1–165) is required for FUS self-association, chromatin binding and transcriptional activation (Yang et al., 2014). CHOP is a member of the CCAAT/enhancer-binding protein (C/EBP) family of transcription factors that play a role in differentiation, proliferation and energy metabolism in various cell types (Hu et al., 2019). Normally, CHOP expression is suppressed, but is upregulated during differentiation and following cellular stress (Ohoka et al., 2007; Yang et al., 2017). In MLS, the fusion protein FUS-CHOP is expressed under the control of the FUS promoter, resulting in ubiquitous expression. Importantly, ubiquitous overexpression of CHOP alone in nude mice does not result in MLS, whereas expression of FUS-CHOP from the same promoter does, indicating that FUS provides novel oncogenic properties to the fusion protein (Perez-Losada et al., 2000).

Genome-wide occupancy analysis of MLS cell lines found that 60% of FUS-CHOP protein maps to putative enhancers, occupying 97% of super enhancers (SEs) defined by the presence of the histone H3 lysine 27 acetylation (H3K27ac) chromatin modification (Chen et al., 2019b). SEs are clusters of transcriptional enhancers that recruit a high density of transcriptional regulators and machinery (Thandapani, 2019). In cancer, SEs can contain numerous mediators, signaling factors, RNA polymerase II and chromatin modifications (such as H3K27ac), which function together as regulators of oncogene expression (Bradner et al., 2017). In liposarcomas, SEs are involved in amplifying cancer pathways, cell migration and angiogenesis (Chen et al., 2019b). A recent hypothesis proposes that liquid–liquid phase separation (LLPS) of protein activators into condensates at SEs can control gene expression (Sabari et al., 2018; Schneider et al., 2021). Such condensation of macromolecules into distinct liquid-phase states – sometimes called membraneless organelles (MLOs) or biomolecular condensates – is attributed to many cellular functions that require spatiotemporal regulation (Banani et al., 2017; Boija et al., 2021). The results of numerous studies suggest that RNA polymerase II, transcription factors, coactivators, SE sequences, mediator proteins (such as MED1) and other transcriptional machinery containing intrinsically disordered regions (IDRs) functionally undergo LLPS at transcriptional start sites, regulating gene expression (Boehning et al., 2018; Boija et al., 2018, 2021; Cho et al., 2018; Crump et al., 2021; Gurumurthy et al., 2019; Lu et al., 2019, 2020; Sabari et al., 2018; Wei et al., 2020).

FUS and the homologous proteins EWS (also known as EWSR1) and TAF15 have been shown to undergo LLPS under several

[1]Department of Biochemistry and Molecular Biology, Uniformed Services University, Bethesda, MD 20814, USA. [2]Center for Biomedical Engineering, Brown University, Providence, RI 02912, USA. [3]Department of Molecular Pharmacology, Physiology, and Biotechnology, Brown University, Providence, RI 02912, USA. [4]Department of Anatomy, Physiology and Genetics, Uniformed Services University, Bethesda, MD 20814, USA. [5]Department of Pharmacology and Molecular Therapeutics, Uniformed Services University, Bethesda, MD 20814, USA.

*Author for correspondence (frank.shewmaker@gmail.com)

I.O., 0000-0002-2417-3673; J.S., 0000-0001-7809-2193; R.K., 0000-0002-1634-4882; N.L.F., 0000-0001-5483-0577; F.S., 0000-0003-2022-0249

Handling Editor: Maria Carmo-Fonseca
Received 24 February 2021; Accepted 24 July 2021

Journal of Cell Science (2021) 134, jcs258578. doi:10.1242/jcs.258578

conditions (Chong et al., 2018; Maharana et al., 2018; Patel et al., 2015) and recruit the C-terminal domain of RNA polymerase II into *in vitro* condensates (Burke et al., 2015). During transcription, FUS and RNA polymerase II are suggested to colocalize into nuclear condensates (Thompson et al., 2018). In an MLS cell line, FUS-CHOP has been found to colocalize at SEs with BRD4 – a protein that is proposed to control gene expression through the formation of phase-separated condensates at SEs (Chen et al., 2019b; Sabari et al., 2018). The N-terminal intrinsically disordered, low-complexity (LC) region (amino acids ∼1–212) of FUS facilitates LLPS in cells and *in vitro* (Burke et al., 2015; Monahan et al., 2017), and importantly, all MLS-causing FUS-CHOP translocations contain portions of this LC sequence (Oikawa et al., 2012; Powers et al., 2010). Similarly, the N-terminal regions of FUS, TAF15 and EWS are all translocated in various forms of sarcomas and leukemias, including Ewing's sarcoma, when fused to any of about a dozen transcription factors (Kovar, 2011). Previous work has shown that FUS-CHOP localizes to nuclear punctate structures, whereas FUS and CHOP individually are diffuse nuclear proteins (Thelin-Jarnum et al., 2002). These punctate structures are eliminated by truncation of the LC region of FUS, thus restoring diffuse localization of FUS-CHOP when large segments of the LC region are removed (Goransson et al., 2002). The FUS-CHOP nuclear puncta have been shown to be distinct from other nuclear bodies, such as promyelocytic leukemia (PML) bodies, but interestingly, Cajal bodies have been shown to localize to the periphery of some of the puncta (Goransson et al., 2002; Thelin-Jarnum et al., 2002). The mechanism by which FUS-CHOP induces oncogenesis remains unknown; however, based on the above observations, we hypothesize that FUS-CHOP has novel phase-separating properties that may induce oncogenesis through condensate formation at transcription sites.

Here, we evaluate the propensity of FUS-CHOP to undergo LLPS *in vitro* and in cells. We assess localization of FUS-CHOP in MLS cancer cell lines and we demonstrate that ectopically expressed FUS-CHOP nuclear puncta have distinct liquid-like characteristics. We also observe FUS-CHOP puncta to colocalize with BRD4, which is a marker of phase-separated SEs (Sabari et al., 2018). Likewise, our results suggest that FUS-CHOP can undergo a liquid-phase transition in the nucleus, which could provide the mechanism for its emergent gain-of-function oncogenicity. This may be a general mechanism for transcriptional activation by fusion oncoproteins that have IDRs.

RESULTS

Recombinant FUS-CHOP undergoes LLPS *in vitro*

Both recombinant full-length FUS and its LC region have previously been shown to undergo LLPS *in vitro* (Burke et al., 2015; Patel et al., 2015). Likewise, droplets formed by the FUS LC region fused to Gal4 have liquid-like dynamics when assessed using fluorescence recovery after photobleaching (FRAP) (Zuo et al., 2021). To determine whether recombinant oncogenic FUS-CHOP can undergo LLPS under similar conditions *in vitro*, we purified the most common type of FUS-CHOP translocation, type II (11 truncation variants of FUS-CHOP have been characterized from patient samples, with the most common being type II and type I; Fig. S1) (Bode-Lesniewska et al., 2007; Oikawa et al., 2012). FUS-CHOP type II contains the first 175 amino acids of FUS fused to full-length CHOP. The transcriptional activation and repression domain, basic region for DNA binding and leucine zipper of CHOP are included in all FUS-CHOP fusions (Fig. 1A; Fig. S1). Using the N-terminal maltose-binding protein (MBP) tag that we have previously used for full-length FUS (Burke et al., 2015; Monahan et al., 2017; Owen et al., 2020), we purified FUS-CHOP type II and CHOP (as a control) from *Escherichia coli* (attempts to purify FUS-CHOP type I were not successful due to insolubility) (Fig. 1A). Similar to our previous observations for wild-type full-length FUS (Burke et al., 2015; Monahan et al., 2017; Owen et al., 2020), upon cleavage of the MBP tag using TEV protease, we observed FUS-CHOP type II droplet formation (Fig. 1B). Concomitant with phase separation, we observed increased turbidity over time for FUS-CHOP type II (Fig. 1C). CHOP alone showed no droplets or marked turbidity after cleavage of the MBP tag, demonstrating that elements within the LC sequence of FUS drive phase separation (Fig. 1B,C). We also assessed FUS-CHOP type II phase separation via turbidity over time with varying salt concentrations (Fig. 1D). The phase behavior of FUS-CHOP was more sensitive to the presence of salt in solution compared to previous observations of full-length FUS. At concentrations of salt above 150 mM, we observed an increase in turbidity, suggesting a decrease in solubility likely due to 'salting out' of the regions that contribute to hydrophobic interactions, similar to that observed with the FUS LC region alone (Burke et al., 2015; Monahan et al., 2017). Overall, these data suggest that the LC domain of FUS provides FUS-CHOP a greater capacity to self-associate and undergo LLPS relative to the unfused CHOP protein.

Ectopically expressed FUS-CHOP–eGFP undergoes LLPS in the nucleus

Previous work has shown that ectopically expressed FUS-CHOP–GFP type II forms distinct nuclear puncta (Thelin-Jarnum et al., 2002). For localization controls, we first ectopically expressed both FUS–eGFP and CHOP–eGFP in NIH 3T3 cells and confirmed diffuse nuclear localization for both proteins (Fig. 2A). We then ectopically expressed FUS-CHOP type I and type II eGFP-tagged fusion proteins (Fig. 2B,C) and observed numerous round nuclear puncta of both the type I and type II constructs (Fig. 2D). To ensure these structures were not the result of the eGFP tag, we also expressed untagged FUS-CHOP type I and type II (Fig. 2C); the untagged proteins formed similar punctate structures (Fig. 2D). Because this nuclear punctate localization pattern of FUS-CHOP was not diffuse like that of either wild-type FUS or CHOP (Fig. 1A), we hypothesized that the puncta are phase-separated condensates driven by the intrinsically disordered LC region of FUS.

Phase-separated condensates in cells are typically characterized by three hallmarks: they are spherical, undergo fusion upon touching, and have rapid internal dynamics and external exchange (Hyman et al., 2014). We used live-cell imaging to assess the puncta in three dimensions. We observed spherical nuclear puncta of FUS-CHOP–eGFP type I and type II (Fig. 3A; Movie 1). Time-lapse imaging of the cells revealed diffuse movement of the puncta, consistent with Brownian motion. We observed occasional fusion events in which two puncta contact each other and subsequently round up (Fig. 3A; Fig. S2, Movie 1). To quantify internal rearrangement and external exchange of FUS-CHOP puncta, we used FRAP (Fig. 3B). Previous work indicates that intracellular liquid-state condensates have half-times of recovery that range from seconds to minutes (Banani et al., 2017). Here, we bleached both type I and type II puncta and observed an average half-time of recovery of ∼19 s and ∼14 s, respectively (Fig. 3C,D). CHOP–eGFP FRAP data were included as a diffuse control. Taken together, these data show that ectopic FUS-CHOP forms nuclear condensates and has the major hallmarks of LLPS.

We also observed that the type I puncta moved more rapidly (they were less static) than the type II puncta. We hypothesize that the RGG repeats present in the longer type I fusion (but not the type II;

Journal of Cell Science (2021) 134, jcs258578. doi:10.1242/jcs.258578

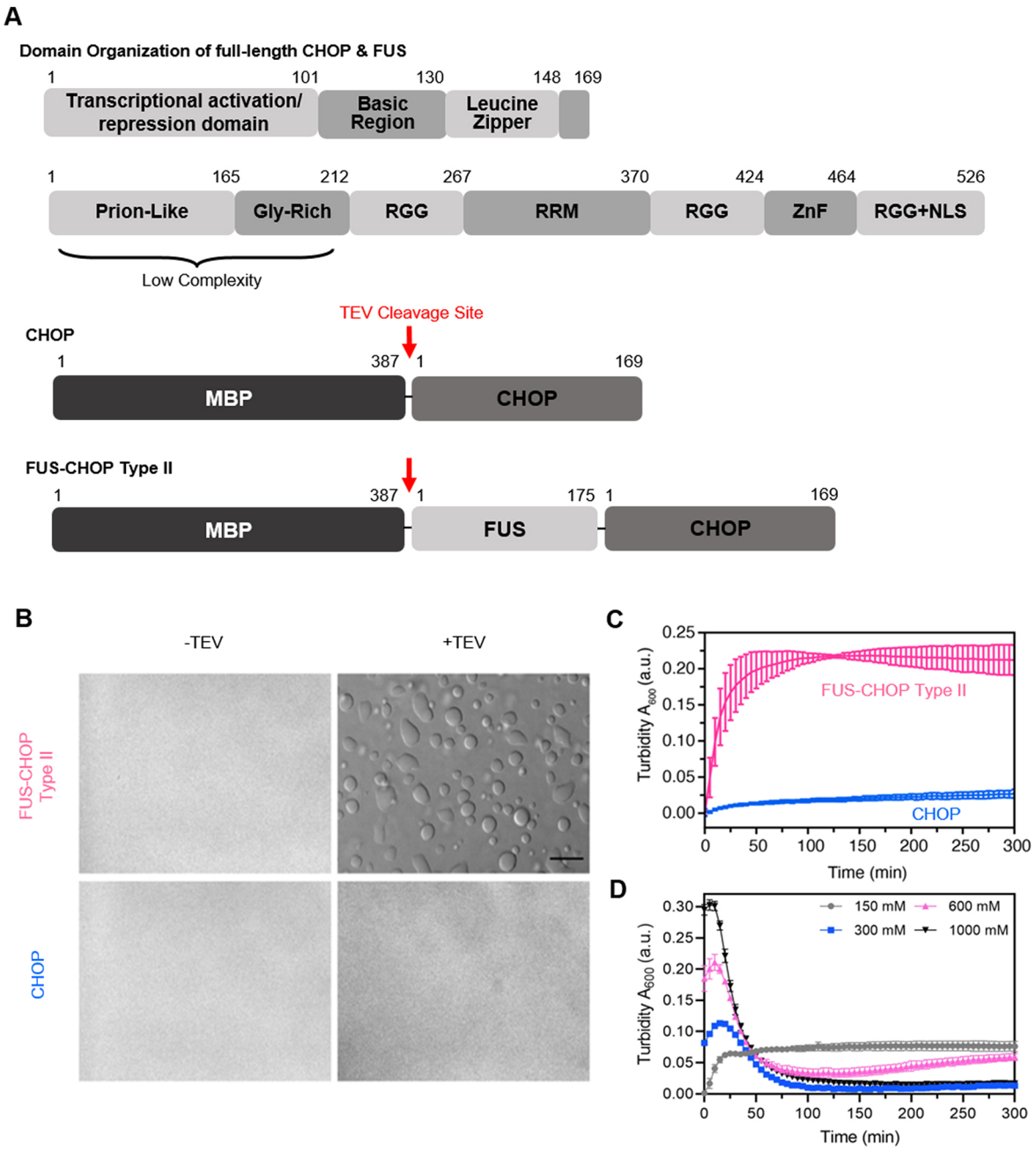

Fig. 1. FUS-CHOP type II undergoes LLPS *in vitro*. (A) Schematic of full-length CHOP (amino acids 1–169) and FUS (amino acids 1–526) as well as purified recombinant MBP–CHOP and MBP–FUS-CHOP. TEV protease cleavage sites are indicated by red arrows. NLS, nuclear localization sequence; RRM, RNA-recognition motif; ZnF, zinc-finger. (B) DIC micrographs of 50 µM FUS-CHOP type II fusion (top) and CHOP protein alone (bottom) in 50 mM Tris-HCl, pH 7.4, and 150 mM NaCl without and with TEV protease to cleave the N-terminal MBP solubilizing tag. Scale bar: 80 µm. (C) Corresponding turbidity measurements (a.u., arbitrary units) of FUS-CHOP type II fusion (pink) and CHOP protein alone (blue) after initiating cleavage of the MBP tag by addition of TEV protease. (D) Turbidity measurements of FUS-CHOP type II fusion at the indicated NaCl concentrations. Data are presented as the mean ±s.d. of measurements from three experimental replicates.

Figs 1A,2B) could be driving additional protein–protein (Ryan et al., 2018; Wang et al., 2018) or protein–RNA interactions (as the LC region does not interact with RNA; Burke et al., 2015), leading to differential mobility throughout the nucleus. However, we did not pursue this observation further.

Phase separation of FUS-CHOP–eGFP is dependent on the FUS PrLD

The FUS LC domain is composed of a PrLD followed by a short glycine-rich region (Fig. 1A), both of which are IDRs with little complexity in their amino acid composition. PrLDs are frequently linked to both LLPS and formation of pathological inclusions in neurodegenerative diseases (March et al., 2016). The FUS PrLD facilitates LLPS of wild-type FUS (Burke et al., 2015), but its truncation inhibits LLPS (Patel et al., 2015). In previously published work, when the PrLD of FUS-CHOP fusions was serially truncated, there was a concomitant dissolution of nuclear puncta (Goransson et al., 2002). To determine the dependence of phase separation on the PrLD (amino acids ∼1–165), we removed the first 25, 50, 75 and 125 amino acids in type I and type II fusion constructs of

Journal of Cell Science (2021) 134, jcs258578. doi:10.1242/jcs.258578

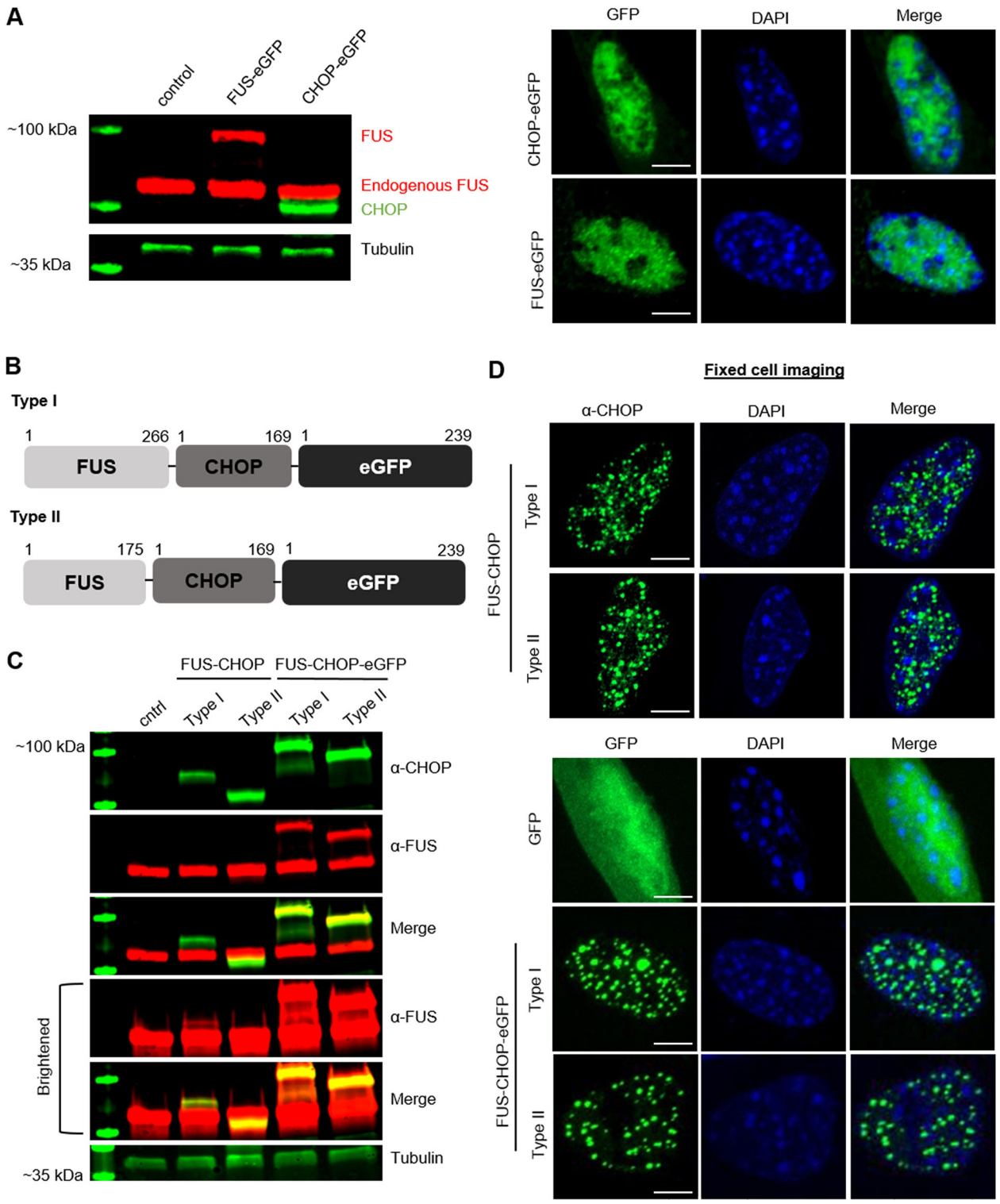

Fig. 2. Ectopically expressed FUS-CHOP localizes to sphere-shaped puncta in the nucleus. (A) Western blot (left) and immunofluorescence images (right) of ectopically expressed FUS–eGFP and CHOP–eGFP. Tubulin is shown as a western blot loading control. (B) Schematic of FUS-CHOP–eGFP fusion proteins. (C) Western blot of ectopically expressed untagged FUS-CHOP and FUS-CHOP–eGFP in NIH 3T3 cells. The bottom panels have been brightened to show all FUS antibody binding. Tubulin is shown as a loading control. (D) Confocal images of nuclear puncta formed by ectopically expressed FUS-CHOP, with (bottom) and without (top) an eGFP tag, in NIH 3T3 cells. GFP alone is shown as a negative control. Scale bars: 5 µm. Representative data from three experimental replicates.

FUS-CHOP–eGFP and expressed the constructs in NIH 3T3 cells (Fig. 4A,B). We observed retention of punctate structures upon removal of up to 50 amino acids (type I is shown in Fig. 4C; identical results for type II are in Fig. S3B). Removing 75 or 125 amino acids resulted in a diffuse pattern of expression, indicating that LLPS is determined by the length of the FUS PrLD (Fig. 4C; Fig. S3).

Journal of Cell Science (2021) 134, jcs258578. doi:10.1242/jcs.258578

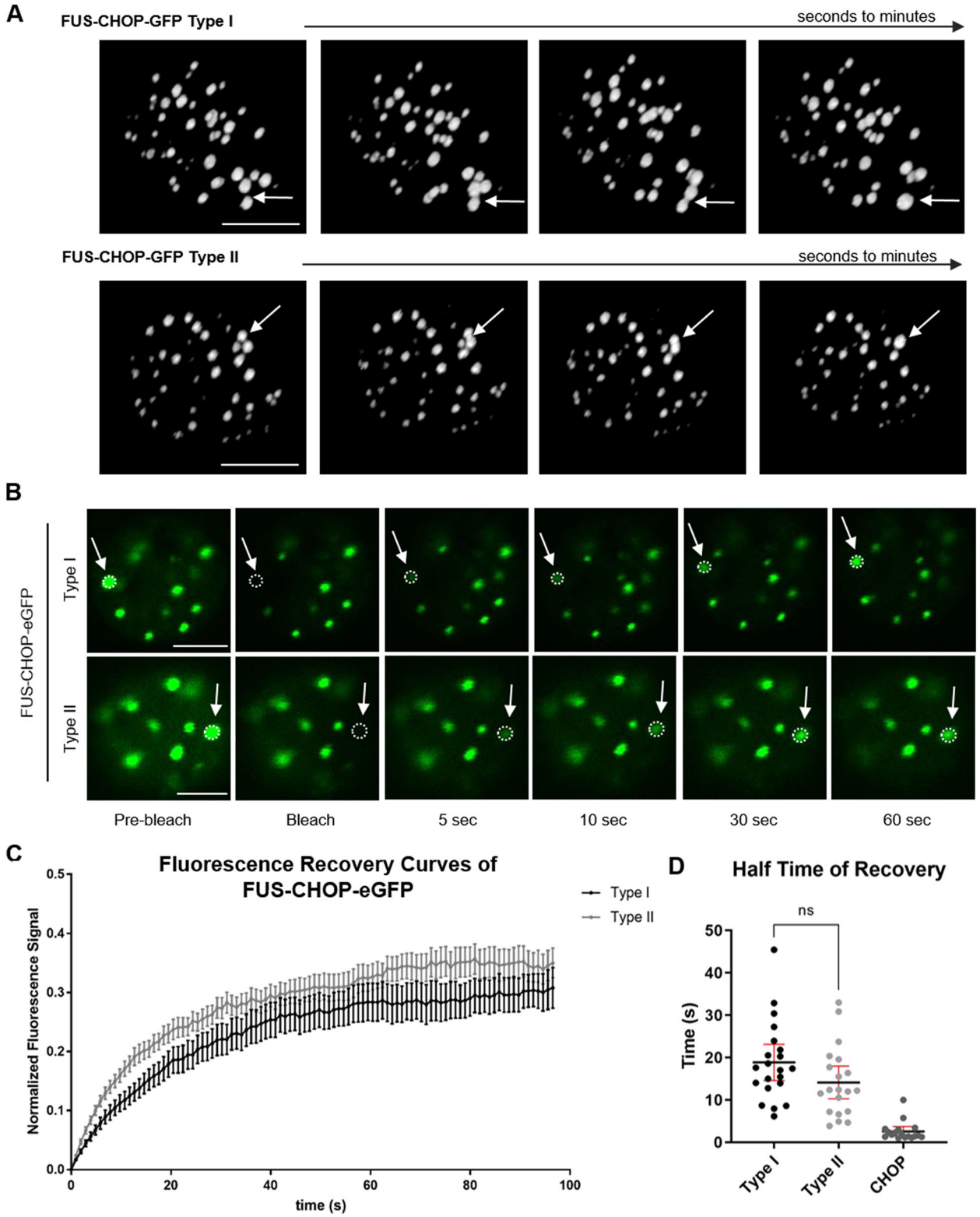

Fig. 3. FUS-CHOP–eGFP puncta have liquid-like characteristics. (A) Frames from timecourse movies of FUS-CHOP–eGFP type I and type II puncta fusing upon touching, imaged using confocal microscopy. Arrows indicate fusion events. Timecourses are shown in Movie 1. (B) FUS-CHOP–eGFP type I and type II puncta recover on the time scale of seconds following fluorescence bleaching. The dashed circles and arrows highlight bleached puncta that undergo fluorescence recovery. Scale bars: 5 µm. Representative data from three experimental replicates. (C) Average fluorescence recovery curves of FUS-CHOP–eGFP type I and type II. (D) Half-time of recovery of FUS-CHOP–eGFP type I and II puncta. FRAP half-time data was statistically analyzed using a two-tailed unpaired *t*-test (P=0.0953; ns, not significant). Data in C and D are presented as the mean±95% c.i. of measurements from three experimental replicates (total of 20 cells bleached per experimental group).

Journal of Cell Science (2021) 134, jcs258578. doi:10.1242/jcs.258578

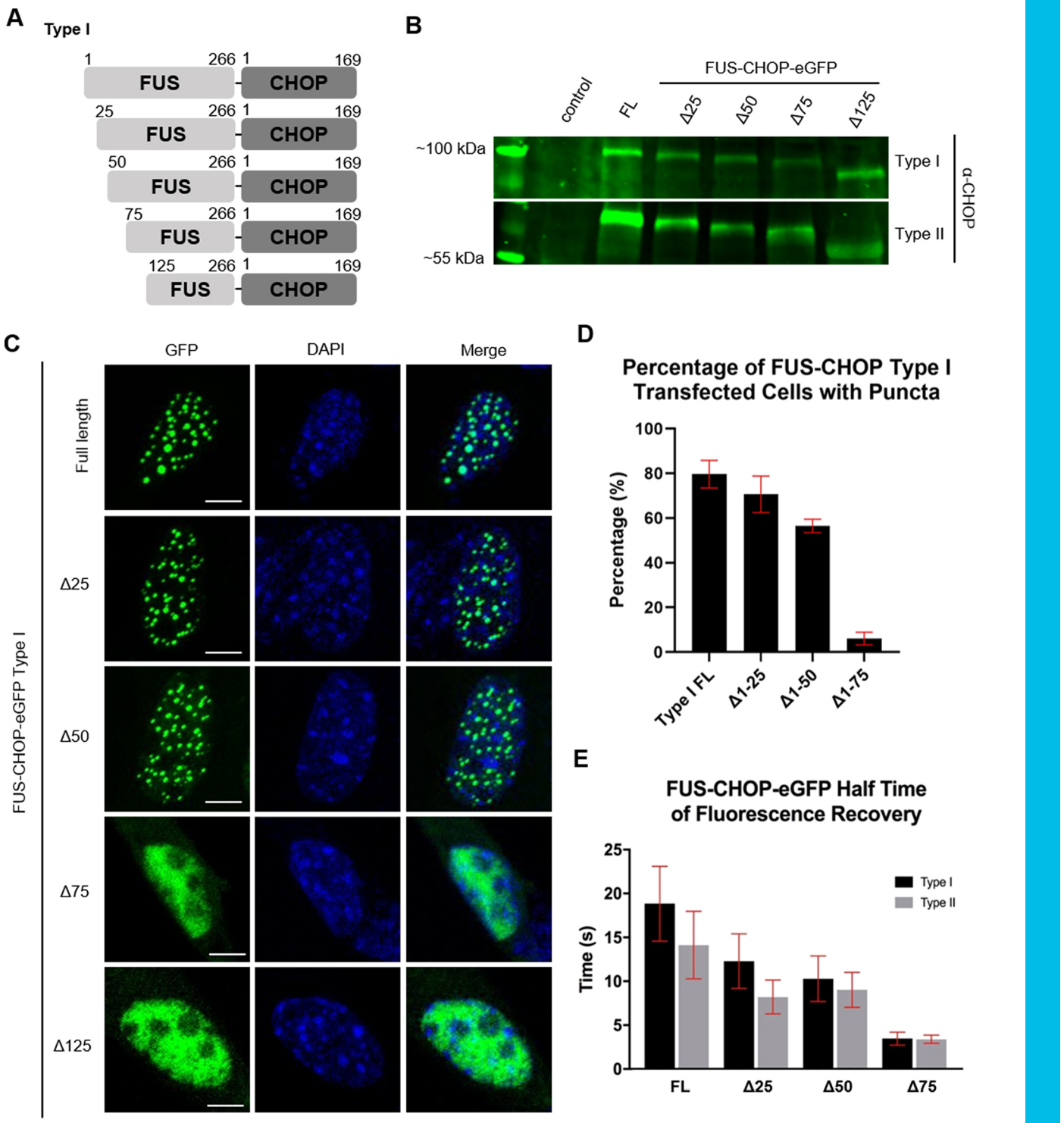

Fig. 4. FUS-CHOP–eGFP liquid–liquid phase separation is dependent on the N terminus of FUS. (A) Schematic of truncations made to FUS-CHOP–eGFP type I. (B) Western blot of NIH 3T3 cells transfected with full-length (FL) FUS-CHOP–eGFP or the indicated truncated FUS-CHOP–eGFP constructs. NIH 3T3 cell lysates were probed with anti-CHOP antibody. Representative data from three experimental replicates. (C) Full-length or truncated FUS-CHOP–eGFP type I ectopically expressed in NIH 3T3 cells and imaged by confocal microscopy. Scale bars: 5 µm. Representative data from three experimental replicates. Images of FUS-CHOP–eGFP type II truncations are shown in Fig. S3. (D) The percentage of eGFP-positive cells containing nuclear puncta were quantified following a 24 h transfection with the indicated constructs. (E) Half-time of recovery of FUS-CHOP–eGFP type I and type II full-length and truncated constructs. Data are presented as the mean±95% c.i. of measurements from three experimental replicates.

Several studies have indicated that tyrosine motifs have an impact on phase-separating proteins (Chong et al., 2018; Lin et al., 2017; Murthy et al., 2019). When ten tyrosine-to-serine mutations are introduced into the EWS-FLI1 fusion protein, a significant reduction of self-association is observed in cells (Chong et al., 2018). Here, a similar trend was observed, as removal of the first 75 amino acids of FUS also removes 11 tyrosine motifs and diminishes FUS-CHOP phase separation. The relationship between the number

Journal of Cell Science (2021) 134, jcs258578. doi:10.1242/jcs.258578

of tyrosine motifs present and phase separation capabilities is consistent with all the truncations utilized in this study (Table S1; Fig. 4). We further characterized how these truncations affected puncta formation by quantifying the percentage of transfected cells with nuclear puncta (Fig. 4D). We observed a decreasing trend of puncta formation with increasing truncation length. To characterize how the PrLD of FUS affects FUS-CHOP LLPS, we used FRAP to quantify recovery time of the truncated proteins within the puncta. We observed a quicker half-time of recovery as the PrLD was shortened, suggesting that length can affect dynamic movement into or within the phase-separated condensate (Fig. 4E). Type I condensates contain more of the FUS N-terminal sequence (266 amino acids) and consistently recover slower than type II condensates (175 amino acids), including the truncated proteins. The length and low-complexity features of the FUS PrLD appear to be the dominant factors in governing FUS-CHOP LLPS, as opposed to any particular sequence element.

The above observation suggests that the interactions driving FUS-CHOP phase separation require most of the PrLD to be intact (see Fig. 1A). These data could point to a special feature or structure in the region spanning residues 51 to 75 of the FUS PrLD; yet, our previous work suggests that the PrLD does not populate specific rigid structures, even in the liquid form (Murthy et al., 2019). Therefore, we also created internal PrLD truncations to test whether the location of the truncation is not important and whether instead the total length of the PrLD present determines phase separation. To this end, we created FUS-CHOP constructs with internal PrLD deletions. We deleted amino acids 50–75, 75–125 and 50–125 in both FUS-CHOP–eGFP type I and type II constructs (Fig. 5A; Fig. S4A) and ectopically expressed them in NIH 3T3 cells to determine their effects on LLPS (Fig. 5B,C; Fig. S4B,C). As with the N-terminal truncations, these constructs were observed to form spherical nuclear punctate structures upon removal of 25 or 50 amino acids (Fig. 5C; Fig. S4C). Removing 75 amino acids within the PrLD resulted predominantly in a pattern of diffuse expression in the nucleus. We quantified the percentage of transfected cells with nuclear puncta and observed the same trend as observed for the N-terminal truncations (Fig. 5D; Fig. S4D).

To determine whether DNA binding is necessary for FUS-CHOP phase separation, we created a previously established DNA-binding mutant lacking the basic region of CHOP (amino acids 101–122; ΔDBD; Fig. 5A) (Ubeda et al., 1996). When FUS-CHOP ΔDBD was expressed in cells, we observed no disruption in nuclear condensate formation (Fig. 5C; Fig. S4C), suggesting that LLPS is not dependent on the DNA-binding ability of CHOP. These data suggest that the PrLD is the main driver of FUS-CHOP–eGFP phase separation, and its length and low-complexity composition determine in-cell phase separation.

FUS-CHOP is localized in small nuclear punctate structures in MLS cell lines

We next sought to characterize endogenous FUS-CHOP in patient-derived cells. We assessed endogenous expression and localization of FUS-CHOP in three different MLS cell lines. MLS-402 and MLS-1765 were both established and immortalized by transfection with SV40 large T antigen, whereas DL-221 was spontaneously immortalized from patient tumor samples (Aman et al., 1992; de Graaff et al., 2016; Thelin-Jarnum et al., 1999). MLS-402 and DL-221 both contain type I fusions, like those we used in ectopic expression, whereas MLS-1765 has a type VIII fusion that encompasses the first 514 amino acids of FUS (Fig. 6A; Fig. S1). All three cell lines showed FUS-CHOP localization to small nuclear punctate structures in every cell, similar to those seen in a previous study evaluating oncogenic EWS-FLI1 fusions in cancer cell lines (Fig. 6B; Movie 2) (Chong et al., 2018). Localization of FUS-CHOP in all cell lines was punctate and nuclear, but expression levels of the type VIII fusion were greater than those of the type I fusions (Fig. 6C). Fixed-cell imaging indicated smaller punctate structures in the cancer cell lines than those observed for the ectopically expressed proteins in NIH 3T3 cells.

SE protein BRD4 localizes with FUS-CHOP

In a previous study, FUS-CHOP was shown to occupy 9% of active promoter sites and 60% of putative enhancer sites in an MLS cell line (Chen et al., 2019b). Using ChIP-seq, the authors found that FUS-CHOP occupied 40% of the same enhancers as BRD4 (Chen et al., 2019b), which itself localizes to enhancer sites marked by acetylated histones (Loven et al., 2013). The authors concluded that FUS-CHOP and BRD4 cooperate at oncogenic SEs in MLS (Chen et al., 2019b). Importantly, BRD4 has an intrinsically disordered C-terminal domain that purportedly drives its phase separation into nuclear puncta at SEs in cell models (Sabari et al., 2018). If FUS-CHOP undergoes LLPS at SEs in our MLS cell lines, then we would predict colocalization with BRD4 at nuclear puncta.

We probed our MLS cancer cell lines for BRD4 puncta and assessed its colocalization with FUS-CHOP (Fig. 7A). The average Pearson's correlation coefficient between BRD4 and FUS-CHOP was 0.440, 0.438 and 0.478 in MLS-1765, MLS-402 and DL221 cell lines, respectively (Fig. 7B). We also evaluated colocalization in our ectopic expression model. We expressed both FUS-CHOP–eGFP type I and type II in NIH 3T3 cells and probed for BRD4 (Fig. 7C). We saw small BRD4 puncta throughout the nucleus in the control, but in the FUS-CHOP–eGFP-expressing cells, BRD4 localized to the large FUS-CHOP–eGFP puncta. The average Pearson's correlation coefficient between BRD4 and FUS-CHOP was 0.688 and 0.780 for type I and type II FUS-CHOP–eGFP, respectively (Fig. 7D). These data suggest that FUS-CHOP and BRD4 occupy the same nuclear condensates at SEs and that FUS-CHOP could be recruiting BRD4 to oncogenic condensates.

To determine the importance of FUS-CHOP DNA binding and BRD4 condensation, we ectopically expressed our FUS-CHOP–eGFP type I and II DNA-binding deficient mutants and probed for BRD4. We observed BRD4 localizing to large FUS-CHOP–eGFP puncta (Fig. 8A). We quantified the Pearson's correlation coefficient between BRD4 and FUS-CHOP–eGFP ΔDBD and observed a significant decrease in colocalization when compared to the colocalization with the full-length counterparts (Fig. 8B). These data suggest that the BRD4 and FUS-CHOP interaction is influenced by DNA binding but is governed by phase separation that is driven by the N-terminus of FUS.

DISCUSSION

Macromolecular condensates that form via LLPS are implicated in many subcellular processes (Alberti and Hyman, 2021). Condensates have recently been proposed to also have roles in pathological events such as oncogenic transcription (Boija et al., 2021). In such cases, oncogenesis would depend on the condensation of transcription factors, mediator complex proteins and chromatin-remodeling proteins to high density at specific SEs and promoter sequences (Boija et al., 2021). Here, we assessed the pathological FUS-CHOP fusion protein – which causes aberrant transcription in MLS (Joseph et al., 2014) – and its capacity to undergo LLPS *in vitro* and in cell models. Our data indicate that N-terminal regions of FUS provide CHOP with novel LLPS properties. In MLS cell lines, we

Journal of Cell Science (2021) 134, jcs258578. doi:10.1242/jcs.258578

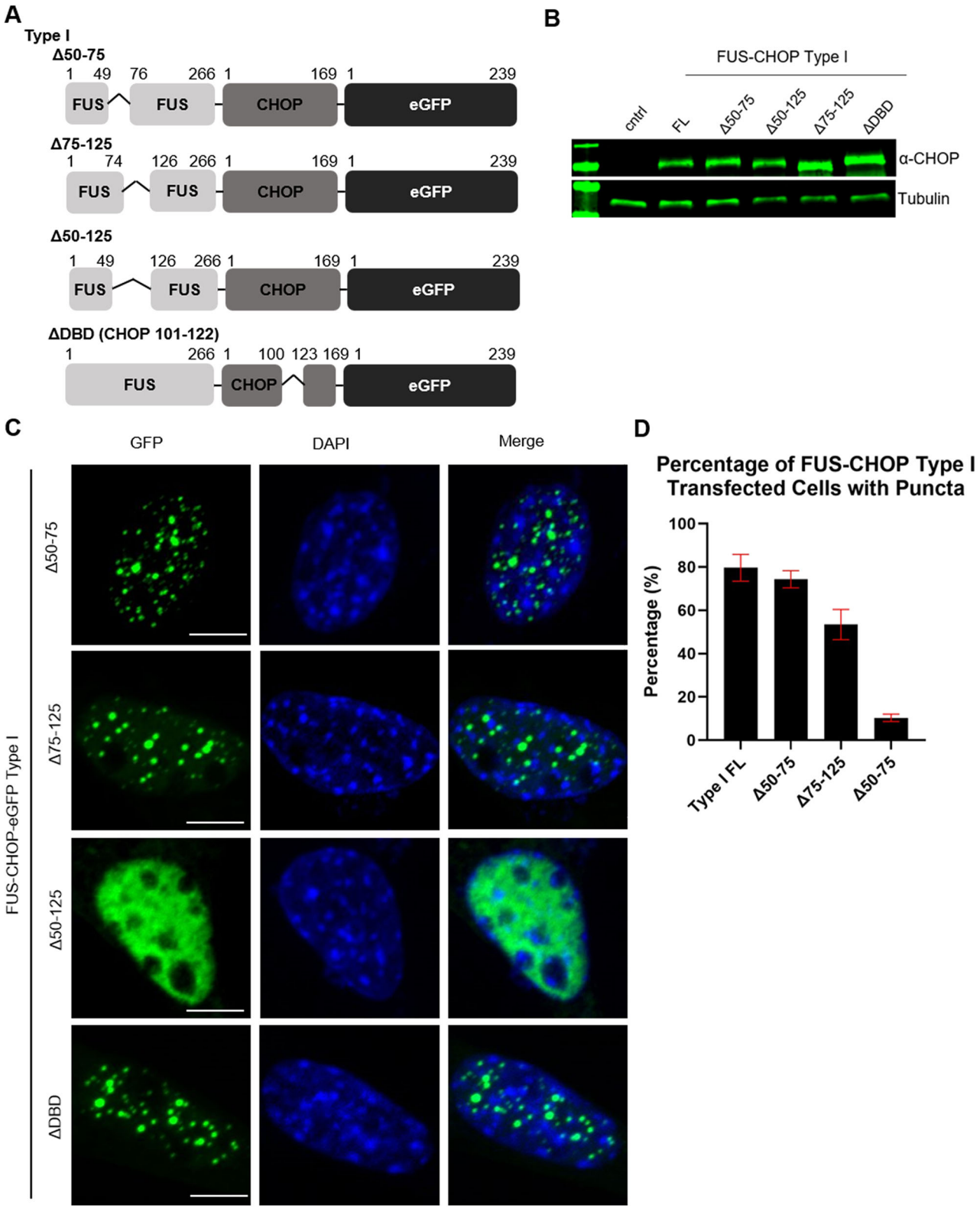

Fig. 5. Phase separation of FUS-CHOP is not dependent on a central core region within the FUS PrLD. (A) Schematic of FUS-CHOP–eGFP type I internal truncations. (B) NIH 3T3 cells transfected with full-length (FL) or truncated (Δ50–75, Δ75–125, Δ50–125 or ΔDBD) FUS-CHOP–eGFP type I constructs. Cell lysates were analyzed by western blot and probed with anti-CHOP and anti-tubulin antibodies. Representative data from three experimental replicates. (C) Confocal images of internally truncated FUS-CHOP–eGFP type I nuclear puncta. Scale bars: 5 µm. Images of FUS-CHOP–eGFP type II truncations are shown in Fig. S4. (D) The percentage of eGFP-positive cells containing nuclear puncta were quantified following a 24 h transfection with the indicated constructs. Data are presented as the mean±95% c.i. of measurements from three experimental replicates.

Journal of Cell Science (2021) 134, jcs258578. doi:10.1242/jcs.258578

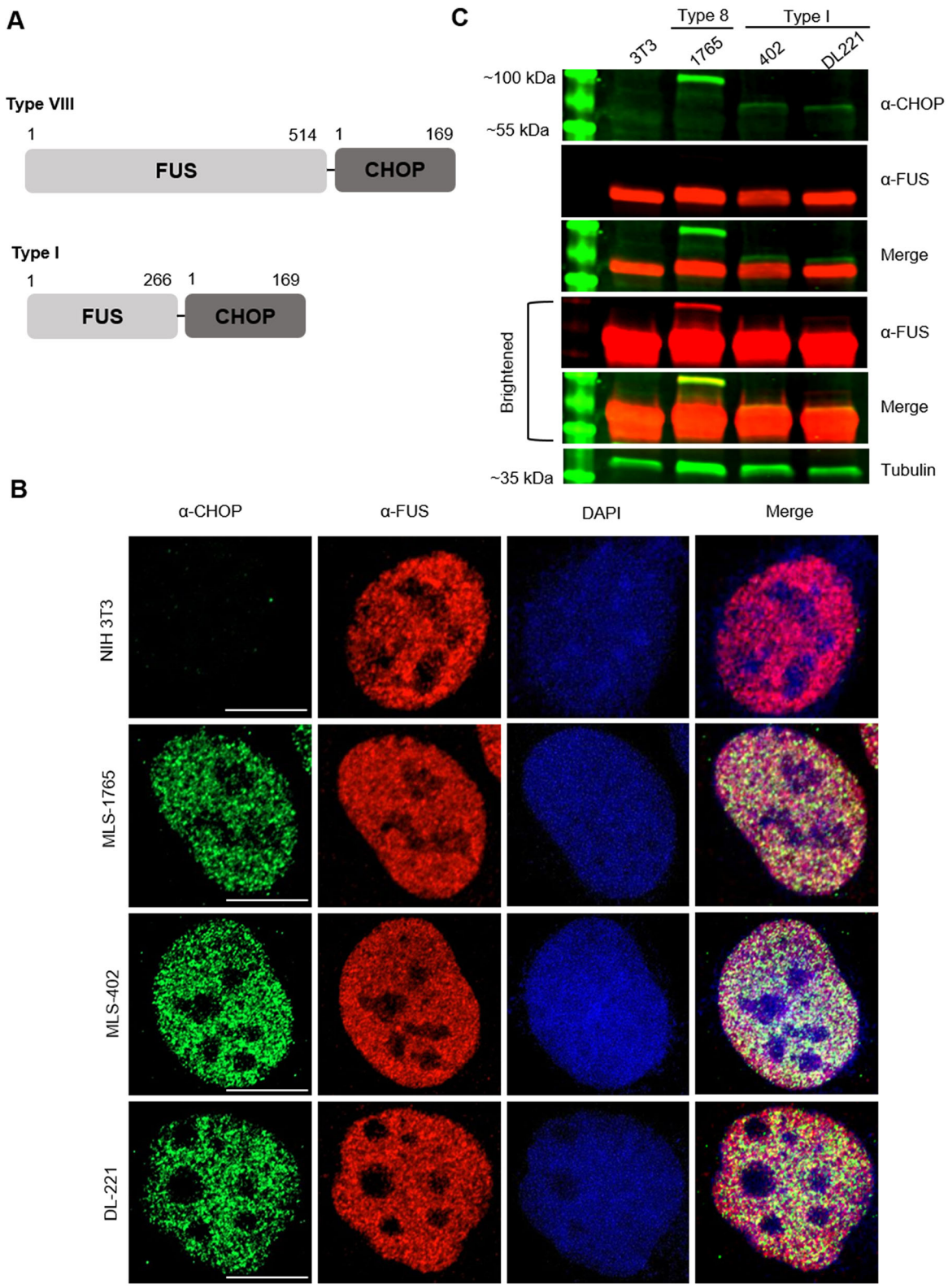

Fig. 6. FUS-CHOP forms nuclear puncta in MLS cell lines. (A) Schematic of FUS-CHOP fusions. MLS-1765 expresses a type VIII FUS-CHOP fusion protein, whereas MLS-402 and DL-221 contain a type I fusion protein (see Fig. S1). (B) MLS cell lines and NIH 3T3 cells were probed with anti-CHOP and anti-FUS antibodies, stained with DAPI and imaged using confocal microscopy with Airyscan. Scale bars: 5 µm. (C) Cancer cell and NIH 3T3 cell lysates analyzed by western blotting with anti-FUS and anti-CHOP antibodies. Brightened blots (bottom) show FUS antibody binding. Tubulin is shown as a loading control. Representative data from three experimental replicates.

Journal of Cell Science (2021) 134, jcs258578. doi:10.1242/jcs.258578

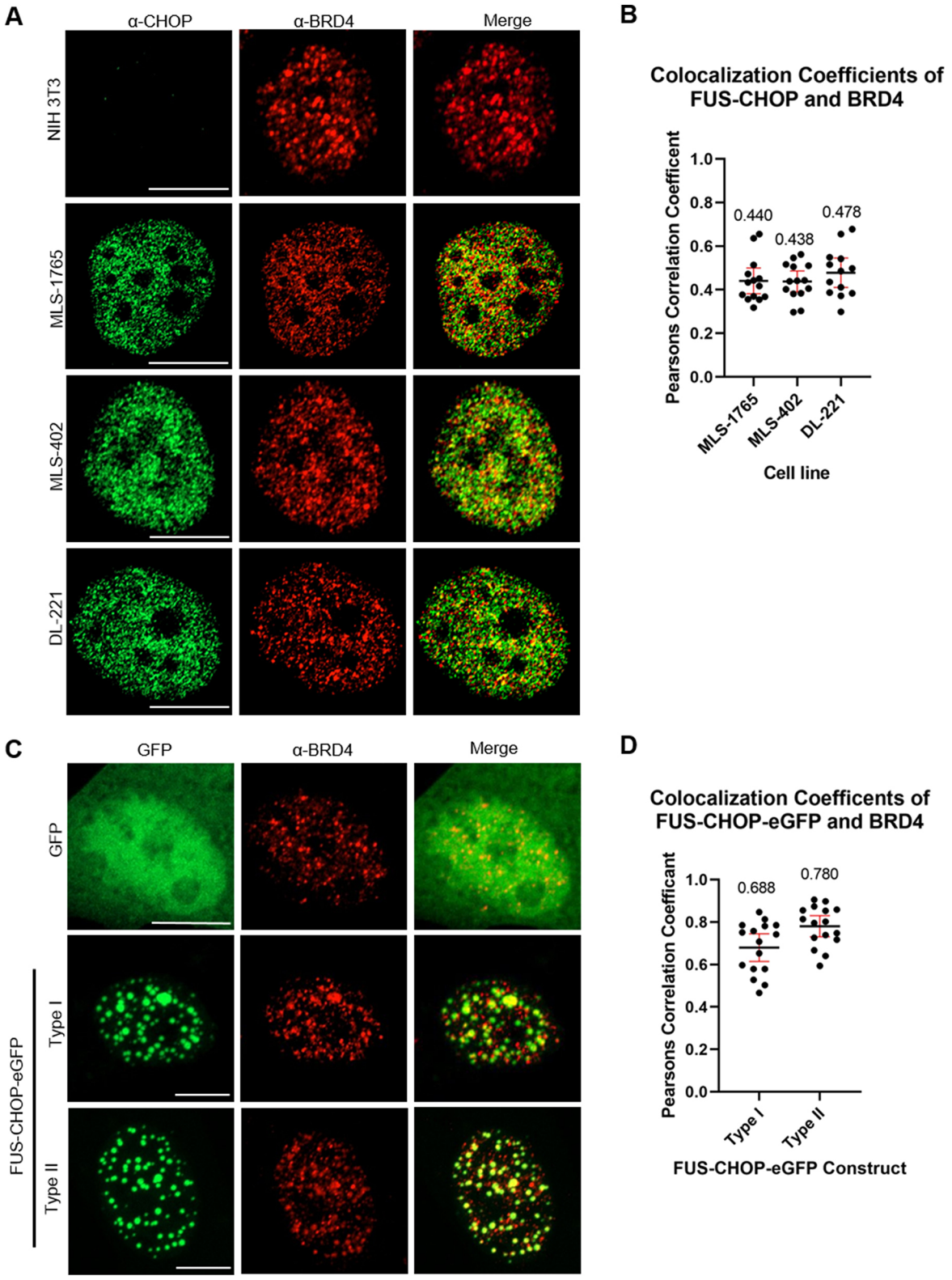

Fig. 7. FUS-CHOP localizes with phase-separating SE protein BRD4. (A) MLS-1765, MLS-402 and DL-221 cells, as well as NIH 3T3 cells, were probed with anti-CHOP and anti-BRD4 antibodies and analyzed by confocal microscopy with Airyscan. Representative data from three experimental replicates. (B) Pearson's correlation coefficient of colocalization between FUS-CHOP and BRD4 in the indicated cell lines was calculated using the EzColocalization plugin in Fiji (total of 13 cells analyzed from each experimental group). (C) NIH 3T3 cells were transfected with FUS-CHOP–eGFP type I or type II, or GFP alone, for 24 h. Following transfection, cells were probed with anti-BRD4 antibody and assessed by confocal microscopy with Airyscan. Representative data from three experimental replicates. (D) Pearson's correlation coefficient of colocalization between FUS-CHOP and BRD4 for the indicated constructs was calculated using the EzColocalization plugin in Fiji (total of 14 cells analyzed from each experimental group). Data in B and D are presented as the mean ±95% c.i., and correlation coefficient values are shown. Scale bars: 5 µm.

Journal of Cell Science (2021) 134, jcs258578. doi:10.1242/jcs.258578

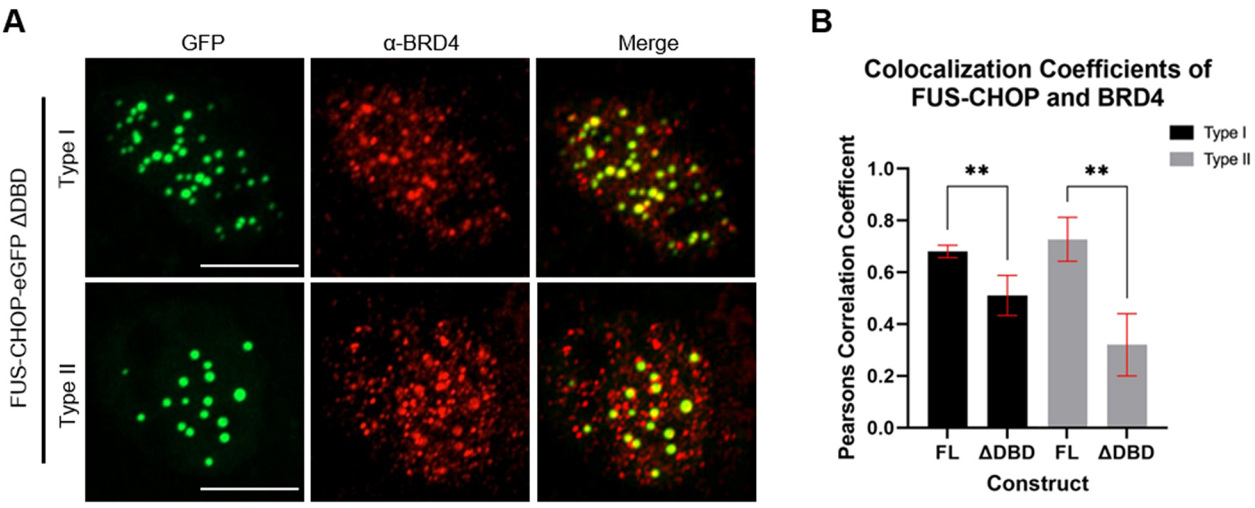

Fig. 8. Phase separation with BRD4 is influenced by FUS-CHOP DNA binding. (A) NIH 3T3 cells were transfected with FUS-CHOP–eGFP type I or type II DNA-binding-deficient mutants for 24 h. Following transfection, cells were probed with anti-BRD4 antibody and assessed using confocal microscopy with Airyscan. Representative data from three experimental replicates. Scale bars: 5 µm. (B) Pearson's correlation coefficient of colocalization between FUS-CHOP and BRD4 was calculated for full-length (FL) FUS-CHOP–eGFP and the DNA-binding-deficient mutants using the EzColocalization plugin in Fiji. Data are presented as the mean±s.d. of measurements from three experimental replicates (total of 14 cells analyzed per experimental group). Colocalization data was statistically analyzed using a two-tailed unpaired *t*-test (type I, P=0.0081; type II, P=0.0031; **P<0.01).

observed the localization of FUS-CHOP condensates at SEs, suggesting that FUS-CHOP LLPS at transcriptional start sites could be integral to oncogenic mechanisms.

FUS is a member of the FET family of proteins, along with EWS and TAF15, which can all undergo LLPS in the nucleus of cells and *in vitro* (Maharana et al., 2018). All three proteins contain an intrinsically disordered, N-terminal PrLD responsible for driving LLPS, and each protein has been found in oncogenic fusions with transcription factors (Linden et al., 2019; Riggi et al., 2007). Under endogenous conditions, the FET family proteins and their fusion partners are mostly diffuse in the nucleus (Andersson et al., 2008). However, as oncogenic fusion proteins, all localize to distinct nuclear puncta (Chong et al., 2018; Thelin-Jarnum et al., 2002). The formation of dysregulated condensates, especially at SEs, is proposed to be an underlying feature of some cancers (Boija et al., 2021). We show that FUS-CHOP can undergo LLPS in the nucleus and form distinct punctate structures with liquid-like dynamics. These condensates could provide an enhanced transcriptional advantage to MLS cells. Concomitant with this study, Zuo et al. corroborated this hypothesis using an *in vitro* transcriptional model. Their data showed the formation of FUS and EWS fusion protein condensates was disrupted with high salt, which then reduced transcriptional output (Zuo et al., 2021). These data suggest that a phase-separating pathological mechanism could be common to FET fusion oncogenic proteins.

The fusion of EWS and the transcription factor FLI1 causes Ewing's sarcoma (Chong et al., 2018). The EWS-FLI1 fusion protein forms condensate-like hubs that are necessary to drive oncogenic transcription (Chong et al., 2018). Here, we see similar results with FUS-CHOP phase separation in the MLS cancer cell lines. To understand how FUS-CHOP might modify the transcriptional landscape in MLS, we looked at the localization of BRD4 – a protein that has been shown to phase separate at SEs. BRD4 has also been shown to colocalize with FUS-CHOP in MLS (Chen et al., 2019b). The C-terminal domain that drives LLPS of BRD4 is necessary for its function (Wang et al., 2019), suggesting that this function could be linked to LLPS. Here, in MLS cancer lines, we observed FUS-CHOP nuclear condensates to colocalize with BRD4. Similarly, in the ectopic expression system, we observed BRD4 localization and consolidation into the large condensates composed of FUS-CHOP–eGFP. This suggests that FUS-CHOP could be driving phase separation of BRD4 at oncogenic SEs in MLS. These findings provide a mechanism by which oncogenic fusion proteins, such as EWS-FLI1 and FUS-CHOP, could hijack BRD4 and other bromodomain-containing proteins to induce oncogenic SEs (Chen et al., 2019b; Gollavilli et al., 2018). FUS-CHOP has also been reported to localize to sites of chromatin remodeling, specifically interacting with the SWI/SNF chromatin-remodeling complex. This interaction is dependent on the FUS PrLD, as truncation eliminates the association (Yu et al., 2019). Taken together, these data suggest a role of FUS-CHOP LLPS in chromatin remodeling and transcription, conferring an oncogenic advantage.

All FUS-CHOP fusion variants that cause MLS contain segments of the FUS PrLD (many also contain longer segments that include the entire LC region, but no fusions lack PrLD segments; Fig. S1). The PrLD drives LLPS of full-length FUS *in vitro* and in cells (Burke et al., 2015; Wang et al., 2018). Our data indicate that the PrLD confers phase-separating capacity to FUS-CHOP. The PrLD is ∼165 residues long, but the induction of LLPS of FUS-CHOP type I and II could still be achieved after truncating the first 50 amino acids from the N terminus. Since the PrLD consists mostly of a few redundant amino acids (SQGY), it does not appear that any sequence feature or motif is required to induce LLPS, but simply a segment of sufficient length. Nearly all characterized FUS-CHOP variants contain the entire PrLD (10 of 11; Fig. S1) (Oikawa et al., 2012), suggesting that shorter fusions are either less probable or less likely to induce MLS transformation. Rare cases of EWS-CHOP fusions have been shown to cause myxoid liposarcoma (Kirsanov et al., 2020; Suzuki et al., 2010). This also suggests that the addition of an IDR to CHOP, which provides phase-separating capabilities, is sufficient to induce oncogenesis, similar to other findings showing IDR replacement approaches (Rawat et al., 2021).

The atomic level structure of condensates appears to be non-static (Burke et al., 2015). However, rigid amyloid-like interactions have been proposed to support the architecture of condensates

Journal of Cell Science (2021) 134, jcs258578. doi:10.1242/jcs.258578

(Kato et al., 2012; Murray et al., 2017). A segment within the PrLD of FUS (residues 39–95) forms a highly ordered amyloid structure in the recombinant protein (Murray et al., 2017). It has been suggested that similar amyloid-like interactions formed by this segment could underlie the structure of the phase-separated state. However, when we deleted an internal portion of the PrLD (residues 75–125), ectopic FUS-CHOP still displayed LLPS properties. This observation suggests that LLPS is a feature that emerges from the low-complexity, intrinsically disordered nature of the PrLD and is not the consequence of a precise sequence element.

Phase separation as a mechanism of transcriptional regulation has not been definitively established (McSwiggen et al., 2019), largely because transcriptional activation sites are small and dynamic, and thus make it challenging to design experiments that strongly support or refute an LLPS hypothesis (McSwiggen et al., 2019). Regardless, LLPS of enhancer-binding proteins, transcription factors and RNA polymerase II at transcriptional sites has been proposed by several groups (Boija et al., 2018; Cho et al., 2018; Hnisz et al., 2017). An LLPS model is attractive because it could explain the low-complexity, intrinsically disordered sequences that are common to transcription factors and coactivators, as these sequences can support multivalent interactions and are prone to phase separation. Our data do not provide information on the molecular-level details of FUS-CHOP-induced transcription in cancer cells. However, our data clearly show that both recombinant and ectopically expressed FUS-CHOP have the capacity to undergo LLPS, whereas this property is not observed for wild-type CHOP under identical conditions. Ectopic expression is imperfect because it may cause proteins to exceed critical concentrations that would not be normally achieved *in vivo* (McSwiggen et al., 2019). If proteins like BRD4 are indeed marking distinct liquid-phase states at transcriptional start sites, then colocalization of FUS-CHOP and the capacity to undergo LLPS suggests that oncogenic transcription patterns could emerge from a phase-separated state. Recently, some cancer drugs have been shown to partition into biomolecular condensates (Klein et al., 2020), and drug concentration within condensates has been shown to influence therapeutic efficacy (Klein et al., 2020). If FUS-CHOP LLPS is integral to oncogenic cellular reprogramming, then this provides a new avenue for pharmacological exploration.

MATERIALS AND METHODS

Cell culture

NIH 3T3 cells (CRL-1658; ATCC, Manassas, VA, USA) were cultured in DMEM (D6429; Sigma-Aldrich, St Louis, MO, USA) supplemented with 10% calf bovine serum (30-2030; ATCC) and 1% penicillin-streptomycin (15140148; Thermo Fisher Scientific, Waltham, MA, USA). DL-221 cells (MD Anderson cell core, Houston, TX, USA) were cultured in DMEM (11875093; Thermo Fisher Scientific) supplemented with 10% fetal bovine serum (F6178; Sigma-Aldrich) and 1% penicillin-streptomycin. MLS402-91 and MLS1765-92 (received from Pierre Åman, University of Gothenburg, Gothenburg, Sweden) were cultured in RPMI (11875093; Thermo Fisher Scientific) supplemented with 10% fetal bovine serum and 1% penicillin-streptomycin. Cells were lysed with a modified RIPA buffer [200 mM NaCl, 100 mM Tris-HCl pH 8, 0.5% sodium deoxycholate, 1% Triton X-100, 670 mM phenylmethylsulfonyl fluoride, 1250 units of benzonase nuclease (E8263; Sigma-Aldrich), 150 µl protease inhibitor cocktail (1861278; Thermo Fisher Scientific) and 100 µl phosphatase inhibitor (78426; Thermo Fisher Scientific)] for 30 min on ice.

Transfections

DNA was transfected into NIH 3T3 cells at ∼70–80% confluency using Lipofectamine 2000 (11668027; Thermo Fisher Scientific) and OptiMEM (31985070; Thermo Fisher Scientific) in a ratio of 3–6 µg DNA to 2.5 µl Lipofectamine 2000 and incubated at 37°C for 24 h unless otherwise stated.

Cloning and plasmids

FUS-CHOP type I and type II genes were synthesized by Genscript (Piscataway, NJ, USA) and subcloned into pcDNA3-EGFP (Addgene 13031; deposited by Doug Golenbock) or 6×His–MBP–FUS FL WT (Addgene 98651; deposited by Nicolas Fawzi) to produce the fusion plasmids. The FUS-CHOP truncations (Δ25, Δ50, Δ75, Δ125 and internal FUS 50–75, 75–125, 50–125 deletions) were generated through PCR cloning using the Phusion High-Fidelity DNA Polymerase (F531S; Thermo Fisher Scientific), designed with either BamHI/Xho or HindIII/BamHI restriction sites. The FUS-CHOP DNA binding Δ101–122 mutants were generated through Q5 site-directed mutagenesis (E0554S; New England BioLabs, Ipswich, MA, USA).

Primer sequences (Integrated DNA Technologies, Coralville, IA, USA) used in the constructs were as follows: FUS forward, 5′-CACAAGCTTA-TGGCCTCAAACGATTATACCCAA-3′; FUS Δ25 forward, 5′-CACGGA-TCCATGTATTCCCAGCAGAGCAG-3′; FUS Δ50 forward, 5′-CACG-GATCCATGTATGGCCAGAGCAGC-3′; FUS Δ75 forward, 5′-CACG-GATCCATGTATGGCTCGACTGGC-3′; FUS Δ125 forward, 5′-CACG-GATCCATGCCCCAGAGTGGGAGC-3′; FUS Δ50 reverse, 5′-GTGG-GATCCGCCTGAAGTGTCCGTGGA-3′; FUS Δ75 reverse, 5′-GAGG-GATCCTCCCTGGGGAGTTGACTGA-3′; eGFP reverse, 5′-TGCTCAC-CATCTCGAG-3′; CHOP Δ101–122 forward, 5′-AAAGAACAGGA-GAATGAAAGG-3′; CHOP Δ101–122 reverse, 5′-CCCTTGGTCTTC-CTCCTC-3′.

Western blotting

Lysates were mixed with 4× NuPAGE LDS Sample Buffer (NP0008; Thermo Fisher Scientific) and electrophoresed through AnyKD precast gels (4569034; Bio-Rad Laboratories, Hercules, CA, USA) at 80 V for 2 h. Gels were transferred using an eBlot L1 (L00686; GenScript) onto nitrocellulose membranes (1620112; Bio-Rad Laboratories). Membranes were blocked with 6% milk (1706404; Bio-Rad Laboratories) in Tris-buffered saline (TBS; J640; VWR International, Radnor, PA, USA). Primary and secondary antibodies were diluted in TBS with 0.1% Tween-20 (P7949; Sigma-Aldrich). The following primary antibodies were used to probe the blots at the indicated dilutions: 1:5000 anti-FUS (A300-302A; Bethyl Laboratories, Montgomery, TX, USA), 1:1000 anti-CHOP (2895S; Cell Signaling Technology, Danvers, MA, USA) and 1:10,000 anti-γ-tubulin (T6557; Sigma-Aldrich). Primary antibodies were detected with secondary antibodies conjugated to 1:20,000 IRDye fluorescent probes (926-68021 and 926-32210; LI-COR Biosciences, Lincoln, NE, USA). Blots were imaged with the Odyssey CLx Imaging System (LI-COR Biosciences). Blot processing was done using Image Studio software (LI-COR Biosciences).

Microscopy

For fixed-cell imaging, cells were grown on glass coverslips for 24 h and fixed with 4% paraformaldehyde (P6148; Sigma-Aldrich). The cells were permeabilized in cold methanol (−20°C) and blocked with 5% normal goat serum (ab7481; Abcam, Cambridge, UK) with 0.05% sodium azide (S2002; Sigma-Aldrich). The following antibodies were used to probe the fixed cells at the indicated dilutions: 1:5000 anti-FUS (A300-302A; Bethyl Laboratories), 1:1000 anti-CHOP (2895S; Cell Signaling Technology) and 1:750 anti-BRD4 (ab128874; Abcam). Secondary antibodies used to detect primary antibodies were used at 1:2500 and were conjugated to either Alexa Fluor AF488 or AF568 (A-11001 and A-11011, respectively; Thermo Fisher Scientific). Nuclei were stained using Prolong mounting medium with DAPI (P36931; Thermo Fisher Scientific). Slides were imaged using Nikon A1R (Melville, NY, USA) and Zeiss 980 with Airyscan (Zeiss, Oberkochen, Germany) microscopes. Airyscan images were taken using the smart setup settings. Images were directly processed using the Zeiss system. All fixed-cell images were further processed using ImageJ (NIH, Bethesda, MD, USA) and Adobe Photoshop. Pearson's correlation coefficient was calculated using the EzColocalization plugin in Fiji (Stauffer et al., 2018).

For live-cell imaging, cells were grown in glass-bottom microwell dishes 24 h prior to transfection. The cells were incubated at 37°C for 24 h post transfection. Before imaging, the medium was changed to dye-free DMEM

(21063029; Thermo Fisher Scientific). To analyze dynamics and fusion events of FUS-CHOP spheres, time-lapse three-dimensional confocal imaging was carried out using the resonant scanner and Piezo *Z*-stage controller of a Nikon A1R microscope. *Z* stacks with an interval of 0.5 µm that encompassed the nucleus of a single cell were acquired every 2 s over a 4 min time period. The *Z* stacks were then processed to generate three-dimensional renderings using Nikon Elements software, and time-lapse renderings were converted to video files. FRAP experiments were also carried out on the Nikon A1R microscope. The center of a granule, marked by a 0.3 µm region of interest, was bleached at 50% power for 1.9 s using the 488 nm laser. The recovery was analyzed for 98 s (∼1.5 min), with image acquisitions every second. The recovery was quantified using the time series analyzer V3 plugin in Fiji. The bleached pixel intensity was subtracted from each data point, and then data points were normalized to the pixel intensity before the bleaching occurred.

In vitro expression and purification of FUS-CHOP fusions and CHOP

N-terminally MBP-tagged (pTHMT) FUS-CHOP fusion type II and CHOP oncogene were expressed in *E, coli* BL21 Star (DE3) cells (C600003; Thermo Fisher Scientific). Bacterial cultures were grown to an optical density at 600 nm of 0.7–0.9 before induction with 1 mM isopropyl-β-D-1-thiogalactopyranoside (IPTG) for 4 h at 37°C. Cell pellets were harvested by centrifugation and stored at −80°C. Cell pellets were resuspended in ∼20 ml of 20 mM sodium phosphate, 1 M NaCl, 10 mM imidazole, pH 7.4, with one Roche EDTA-free protease inhibitor tablet (11697498001; Sigma-Aldrich) for ∼2 g cell pellet, and lysed using the Avestin Emulsiflex C3 (Ottawa, Ontario, Canada). The lysate was cleared by centrifugation at 47,850 ***g*** for 50 min at 4°C, filtered using a 0.2 µm syringe filter, and loaded onto a HisTrap HP 5 ml column (17524701; Cytiva, Marlborough, MA, USA). The protein was eluted with a gradient from 10 to 300 mM imidazole in 20 mM sodium phosphate, 1 M NaCl, pH 7.4. Fractions containing MBP-tagged FUS-CHOP fusion type II or CHOP were loaded onto a HiLoad 26/600 Superdex 200 pg column (28-9893-36; Cytiva) equilibrated in 20 mM sodium phosphate and 1.0 M NaCl. Fractions with high purity were identified by SDS–PAGE and concentrated using a centrifugation filter with a 10 kDa cutoff (ACS501024; MilliporeSigma, Burlington, MA, USA). MBP–FUS-CHOP fusion type II and MBP–CHOP proteins were then flash frozen in 25% glycerol.

Turbidity measurements

Turbidity was used to evaluate phase separation of 50 µM MBP–FUS-CHOP fusion type II and MBP–CHOP in the presence of 0.01 mg ml^{-1} TEV protease (∼0.3 mg ml^{-1} in 50 mM Tris-HCl, pH 7.5, 1 mM EDTA, 5 mM dithiothreitol, 50% glycerol and 0.1% Triton X-100). The experiment was performed in 50 mM Tris-HCl, pH 7.4 and 150 mM NaCl. Turbidity experiments were performed in a 96-well clear plate with 70 µl samples sealed with optical adhesive film to prevent evaporation (4311971; Thermo Fisher Scientific). The absorbance at 600 nm (A_{600}) was monitored over time using a Cytation 5 Cell Imaging Multi-Mode Reader (BioTek Instruments, Winooski, VT, USA) at 5 min time intervals for up to 12 h with mixing and subtracted from a blank buffer with no turbidity.

Differential interference contrast microscopy

For 50 µM MBP–FUS-CHOP type II fusion and MBP–CHOP, the samples were incubated with 0.03 mg ml^{-1} TEV protease for ∼20 min before visualization. Samples were spotted onto a glass coverslip, and droplet formation was evaluated by imaging with differential interference contrast (DIC) on an Axiovert 200M microscope (Zeiss).

Acknowledgements

We thank Dennis McDaniel for his assistance with confocal microscopy. We also thank Pierre Åman for sharing the myxoid liposarcoma cell lines with our lab.

Competing interests

The authors declare no competing or financial interests.

Author contributions

Conceptualization: I.O., D.Y., F.S.; Methodology: I.O., D.Y., J.S., N.L.F., F.S.; Validation: I.O.; Formal analysis: I.O., D.Y., F.S.; Investigation: I.O., D.Y., T.M.P., V.J., F.S.; Resources: I.O., D.Y., H.W., R.K., N.L.F., F.S.; Data curation: I.O., D.Y., T.M.P., V.J., F.S.; Writing - original draft: I.O., D.Y., N.L.F., F.S.; Writing - review & editing: I.O., D.Y., H.W., J.S., R.K., N.L.F., F.S.; Visualization: I.O.; Supervision: N.L.F., F.S.; Project administration: N.L.F., F.S.; Funding acquisition: N.L.F., F.S.

Funding

This project was supported by the National Institute of General Medical Sciences (R35GM119790 to F.S. and R01GM118530 to N.L.F.) and the National Institute of Neurological Diseases and Stroke (R01NS116176 to N.L.F.). Deposited in PMC for release after 12 months.

Peer review history

The peer review history is available online at https://journals.biologists.com/jcs/article-lookup/doi/10.1242/jcs.258578

References

Alberti, S. and Hyman, A. A. (2021). Biomolecular condensates at the nexus of cellular stress, protein aggregation disease and ageing. *Nat. Rev. Mol. Cell Biol.* **22**, 196-213. doi:10.1038/s41580-020-00326-6

Åman, P., Ron, D., Mandahl, N., Fioretos, T., Heim, S., Arheden, K., Willén, H., Rydholm, A. and Mitelman, F. (1992). Rearrangement of the transcription factor gene CHOP in myxoid liposarcomas with t(12;16)(q13;p11). *Genes Chromosomes Cancer* **5**, 278-285. doi:10.1002/gcc.2870050403

Andersson, M. K., Ståhlberg, A., Arvidsson, Y., Olofsson, A., Semb, H., Stenman, G., Nilsson, O. and Åman, P. (2008). The multifunctional FUS, EWS and TAF15 proto-oncoproteins show cell type-specific expression patterns and involvement in cell spreading and stress response. *BMC Cell Biol.* **9**, 37. doi:10.1186/1471-2121-9-37

Banani, S. F., Lee, H. O., Hyman, A. A. and Rosen, M. K. (2017). Biomolecular condensates: organizers of cellular biochemistry. *Nat. Rev. Mol. Cell Biol.* **18**, 285-298. doi:10.1038/nrm.2017.7

Bock, S., Hoffmann, D. G., Jiang, Y., Chen, H. and Il'yasova, D. (2020). Increasing incidence of liposarcoma: a population-based study of national surveillance databases, 2001–2016. *Int. J. Environ. Res. Public Health* **17**, 2710. doi:10.3390/ijerph17082710

Bode-Lesniewska, B., Frigerio, S., Exner, U., Abdou, M. T., Moch, H. and Zimmermann, D. R. (2007). Relevance of translocation type in myxoid liposarcoma and identification of a novel EWSR1-DDIT3 fusion. *Genes Chromosomes Cancer* **46**, 961-971. doi:10.1002/gcc.20478

Boehning, M., Dugast-Darzacq, C., Rankovic, M., Hansen, A. S., Yu, T., Marie-Nelly, H., McSwiggen, D. T., Kokic, G., Dailey, G. M., Cramer, P. et al. (2018). RNA polymerase II clustering through carboxy-terminal domain phase separation. *Nat. Struct. Mol. Biol.* **25**, 833-840. doi:10.1038/s41594-018-0112-y

Boija, A., Klein, I. A., Sabari, B. R., Dall'Agnese, A., Coffey, E. L., Zamudio, A. V., Li, C. H., Shrinivas, K., Manteiga, J. C., Hannett, N. M. et al. (2018). Transcription factors activate genes through the phase-separation capacity of their activation domains. *Cell* **175**, 1842-1855.e16. doi:10.1016/j.cell.2018.10.042

Boija, A., Klein, I. A. and Young, R. A. (2021). Biomolecular condensates and cancer. *Cancer Cell* **39**, 174-192. doi:10.1016/j.ccell.2020.12.003

Bradner, J. E., Hnisz, D. and Young, R. A. (2017). Transcriptional addiction in cancer. *Cell* **168**, 629-643. doi:10.1016/j.cell.2016.12.013

Burke, K. A., Janke, A. M., Rhine, C. L. and Fawzi, N. L. (2015). Residue-by-residue view of in vitro FUS granules that bind the C-terminal domain of RNA Polymerase II. *Mol. Cell* **60**, 231-241. doi:10.1016/j.molcel.2015.09.006

Chen, C., Ding, X., Akram, N., Xue, S. and Luo, S.-Z. (2019a). Fused in sarcoma: properties, self-assembly and correlation with neurodegenerative diseases. *Molecules* **24**, 1622. doi:10.3390/molecules24081622

Chen, Y., Xu, L., Mayakonda, A., Huang, M.-L., Kanojia, D., Tan, T. Z., Dakle, P., Lin, R. Y.-T., Ke, X.-Y., Said, J. W. et al. (2019b). Bromodomain and extraterminal proteins foster the core transcriptional regulatory programs and confer vulnerability in liposarcoma. *Nat. Commun.* **10**, 1353. doi:10.1038/s41467-019-09257-z

Cho, W.-K., Spille, J.-H., Hecht, M., Lee, C., Li, C. and Grube, V. and Cisse, I. I. (2018). Mediator and RNA polymerase II clusters associate in transcription-dependent condensates. *Science* **361**, 412-415. doi:10.1126/science.aar4199

Chong, S., Dugast-Darzacq, C., Liu, Z., Dong, P., Dailey, G. M., Cattoglio, C., Heckert, A., Banala, S., Lavis, L., Darzacq, X. et al. (2018). Imaging dynamic and selective low-complexity domain interactions that control gene transcription. *Science* **361**, eaar2555. doi:10.1126/science.aar2555

Crump, N. T., Ballabio, E., Godfrey, L., Thorne, R., Repapi, E., Kerry, J., Tapia, M., Hua, P., Lagerholm, C., Filippakopoulos, P. et al. (2021). BET inhibition disrupts transcription but retains enhancer-promoter contact. *Nat. Commun.* **12**, 223. doi:10.1038/s41467-020-20400-z

de Graaff, M. A., Yu, J. S. E., Beird, H. C., Ingram, D. R., Nguyen, T., Juehui Liu, J., Bolshakov, S., Szuhai, K., Åman, P., Torres, K. E. et al. (2016).

Establishment and characterization of a new human myxoid liposarcoma cell line (DL-221) with the FUS-DDIT3 translocation. *Lab. Invest.* **96**, 885-894. doi:10.1038/labinvest.2016.64

Gollavilli, P. N., Pawar, A., Wilder-Romans, K., Natesan, R., Engelke, C. G., Dommeti, V. L., Krishnamurthy, P. M., Nallasivam, A., Apel, I. J., Xu, T. et al. (2018). EWS/ETS-driven ewing sarcoma requires BET bromodomain proteins. *Cancer Res.* **78**, 4760-4773. doi:10.1158/0008-5472.CAN-18-0484

Göransson, M., Wedin, M. and Åman, P. (2002). Temperature-dependent localization of TLS-CHOP to splicing factor compartments. *Exp. Cell Res.* **278**, 125-132. doi:10.1006/excr.2002.5566

Gurumurthy, A., Shen, Y., Gunn, E. M. and Bungert, J. (2019). Phase separation and transcription regulation: are super-enhancers and locus control regions primary sites of transcription complex assembly? *BioEssays* **41**, 1800164. doi:10.1002/bies.201800164

Hnisz, D., Shrinivas, K., Young, R. A., Chakraborty, A. K. and Sharp, P. A. (2017). A phase separation model for transcriptional control. *Cell* **169**, 13-23. doi:10.1016/j.cell.2017.02.007

Hu, H., Tian, M., Ding, C. and Yu, S. (2019). The C/EBP Homologous Protein (CHOP) transcription factor functions in endoplasmic reticulum stress-induced apoptosis and microbial infection. *Front. Immunol.* **9**, 3083. doi:10.3389/fimmu.2018.03083

Hyman, A. A., Weber, C. A. and Jülicher, F. (2014). Liquid-liquid phase separation in biology. *Annu. Rev. Cell Dev. Biol.* **30**, 39-58. doi:10.1146/annurev-cellbio-100913-013325

Joseph, C. G., Hwang, H., Jiao, Y., Wood, L. D., Kinde, I., Wu, J., Mandahl, N., Luo, J., Hruban, R. H., Diaz, L. A.Jr. et al. (2014). Exomic analysis of myxoid liposarcomas, synovial sarcomas, and osteosarcomas. *Genes Chromosomes Cancer* **53**, 15-24. doi:10.1002/gcc.22114

Kato, M., Han, T. W., Xie, S., Shi, K., Du, X., Wu, L. C., Mirzaei, H., Goldsmith, E. J., Longgood, J., Pei, J. et al. (2012). Cell-free formation of RNA granules: low complexity sequence domains form dynamic fibers within hydrogels. *Cell* **149**, 753-767. doi:10.1016/j.cell.2012.04.017

Kirsanov, K. I., Lesovaya, E. A., Fetisov, T. I., Bokhyan, B. Y., Belitsky, G. A. and Yakubovskaya, M. G. (2020). Current approaches for personalized therapy of soft tissue sarcomas. *Sarcoma* **2020**, 6716742. doi:10.1155/2020/6716742

Klein, I. A., Boija, A., Afeyan, L. K., Hawken, S. W., Fan, M., Dall'Agnese, A., Oksuz, O., Henninger, J. E., Shrinivas, K., Sabari, B. R. et al. (2020). Partitioning of cancer therapeutics in nuclear condensates. *Science* **368**, 1386-1392. doi:10.1126/science.aaz4427

Kovar, H. (2011). Dr. Jekyll and Mr. Hyde: the two faces of the FUS/EWS/TAF15 protein family. *Sarcoma* **2011**, 837474. doi:10.1155/2011/837474

Lin, Y., Currie, S. L. and Rosen, M. K. (2017). Intrinsically disordered sequences enable modulation of protein phase separation through distributed tyrosine motifs. *J. Biol. Chem.* **292**, 19110-19120. doi:10.1074/jbc.M117.800466

Lindén, M., Thomsen, C., Grundevik, P., Jonasson, E., Andersson, D., Runnberg, R., Dolatabadi, S., Vannas, C., Luna Santamaríotaa, M., Fagman, H. et al. (2019). FET family fusion oncoproteins target the SWI/SNF chromatin remodeling complex. *EMBO Rep.* **20**, e45766. doi:10.15252/embr.201845766

Lovén, J., Hoke, H. A., Lin, C. Y., Lau, A., Orlando, D. A., Vakoc, C. R., Bradner, J. E., Lee, T. I. and Young, R. A. (2013). Selective inhibition of tumor oncogenes by disruption of super-enhancers. *Cell* **153**, 320-334. doi:10.1016/j.cell.2013.03.036

Lu, H., Liu, R. and Zhou, Q. (2019). Balanced between order and disorder: a new phase in transcription elongation control and beyond. *Transcription* **10**, 157-163. doi:10.1080/21541264.2019.1570812

Lu, Y., Wu, T., Gutman, O., Lu, H., Zhou, Q., Henis, Y. I. and Luo, K. (2020). Phase separation of TAZ compartmentalizes the transcription machinery to promote gene expression. *Nat. Cell Biol.* **22**, 453-464. doi:10.1038/s41556-020-0485-0

Maharana, S., Wang, J., Papadopoulos, D. K., Richter, D., Pozniakovsky, A., Poser, I., Bickle, M., Rizk, S., Guillén-Boixet, J., Franzmann, T. M. et al. (2018). RNA buffers the phase separation behavior of prion-like RNA binding proteins. *Science* **360**, 918-921. doi:10.1126/science.aar7366

March, Z. M., King, O. D. and Shorter, J. (2016). Prion-like domains as epigenetic regulators, scaffolds for subcellular organization, and drivers of neurodegenerative disease. *Brain Res.* **1647**, 9-18. doi:10.1016/j.brainres.2016.02.037

McSwiggen, D. T., Mir, M., Darzacq, X. and Tjian, R. (2019). Evaluating phase separation in live cells: diagnosis, caveats, and functional consequences. *Genes Dev.* **33**, 1619-1634. doi:10.1101/gad.331520.119

Monahan, Z., Ryan, V. H., Janke, A. M., Burke, K. A., Rhoads, S. N., Zerze, G. H., O'Meally, R., Dignon, G. L., Conicella, A. E., Zheng, W. et al. (2017). Phosphorylation of the FUS low-complexity domain disrupts phase separation, aggregation, and toxicity. *EMBO J.* **36**, 2951-2967. doi:10.15252/embj.201696394

Murray, D. T., Kato, M., Lin, Y., Thurber, K. R., Hung, I., McKnight, S. L. and Tycko, R. (2017). Structure of FUS protein fibrils and its relevance to self-assembly and phase separation of low-complexity domains. *Cell* **171**, 615-627.e16. doi:10.1016/j.cell.2017.08.048

Murthy, A. C., Dignon, G. L., Kan, Y., Zerze, G. H., Parekh, S. H., Mittal, J. and Fawzi, N. L. (2019). Molecular interactions underlying liquid-liquid phase separation of the FUS low-complexity domain. *Nat. Struct. Mol. Biol.* **26**, 637-648. doi:10.1038/s41594-019-0250-x

Ohoka, N., Hattori, T., Kitagawa, M., Onozaki, K. and Hayashi, H. (2007). Critical and functional regulation of CHOP (C/EBP homologous protein) through the N-terminal portion. *J. Biol. Chem.* **282**, 35687-35694. doi:10.1074/jbc.M703735200

Oikawa, K., Tanaka, M., Itoh, S., Takanashi, M., Ozaki, T., Muragaki, Y. and Kuroda, M. (2012). A novel oncogenic pathway by TLS-CHOP involving repression of MDA-7/IL-24 expression. *Br. J. Cancer* **106**, 1976-1979. doi:10.1038/bjc.2012.199

Owen, I., Rhoads, S., Yee, D., Wyne, H., Gery, K., Hannula, I., Sundrum, M. and Shewmaker, F. (2020). The prion-like domain of Fused in Sarcoma is phosphorylated by multiple kinases affecting liquid- and solid-phase transitions. *Mol. Biol. Cell* **31**, 2522-2536. doi:10.1091/mbc.E20-05-0290

Patel, A., Lee, H. O., Jawerth, L., Maharana, S., Jahnel, M., Hein, M. Y., Stoynov, S., Mahamid, J., Saha, S., Franzmann, T. M. et al. (2015). A liquid-to-solid phase transition of the ALS protein FUS accelerated by disease mutation. *Cell* **162**, 1066-1077. doi:10.1016/j.cell.2015.07.047

Pérez-Losada, J., Sánchez-Martín, M., Rodríguez-García, M. A., Pérez-Mancera, P. A., Pintado, B., Flores, T., Battaner, E. and Sánchez-García, I. (2000). Liposarcoma initiated by FUS/TLS-CHOP: the FUS/TLS domain plays a critical role in the pathogenesis of liposarcoma. *Oncogene* **19**, 6015-6022. doi:10.1038/sj.onc.1204018

Powers, M. P., Wang, W.-L., Hernandez, V. S., Patel, K. S., Lev, D. C., Lazar, A. J. and López-Terrada, D. H. (2010). Detection of myxoid liposarcoma-associated FUS-DDIT3 rearrangement variants including a newly identified breakpoint using an optimized RT-PCR assay. *Mod. Pathol.* **23**, 1307-1315. doi:10.1038/modpathol.2010.118

Rawat, P., Boehning, M., Hummel, B., Aprile-Garcia, F., Pandit, A. S., Eisenhardt, N., Khavaran, A., Niskanen, E., Vos, S. M., Palvimo, J. J. et al. (2021). Stress-induced nuclear condensation of NELF drives transcriptional downregulation. *Mol. Cell* **81**, 1013-1026.e11. doi:10.1016/j.molcel.2021.01.016

Riggi, N., Cironi, L., Suvà, M.-L. and Stamenkovic, I. (2007). Sarcomas: genetics, signalling, and cellular origins. Part 1: the fellowship of TET. *J. Pathol.* **213**, 4-20. doi:10.1002/path.2209

Ryan, V. H., Dignon, G. L., Zerze, G. H., Chabata, C. V., Silva, R., Conicella, A. E., Amaya, J., Burke, K. A., Mittal, J. and Fawzi, N. L. (2018). Mechanistic view of hnRNPA2 low-complexity domain structure, interactions, and phase separation altered by mutation and arginine methylation. *Mol. Cell* **69**, 465-479.e7. doi:10.1016/j.molcel.2017.12.022

Sabari, B. R., Dall'Agnese, A., Boija, A., Klein, I. A., Coffey, E. L., Shrinivas, K., Abraham, B. J., Hannett, N. M., Zamudio, A. V., Manteiga, J. C. et al. (2018). Coactivator condensation at super-enhancers links phase separation and gene control. *Science* **361**, eaar3958. doi:10.1126/science.aar3958

Schneider, N., Wieland, F. G., Kong, D., Fischer, A. A. M., Hörner, M., Timmer, J., Ye, H. and Weber, W. (2021). Liquid-liquid phase separation of light-inducible transcription factors increases transcription activation in mammalian cells and mice. *Sci. Adv.* **7**, eabd3568. doi:10.1126/sciadv.abd3568

Siegel, R. L., Miller, K. D. and Jemal, A. (2015). Cancer statistics, 2015. *CA Cancer J. Clin.* **65**, 5-29. doi:10.3322/caac.21254

Stauffer, W., Sheng, H. and Lim, H. N. (2018). EzColocalization: an ImageJ plugin for visualizing and measuring colocalization in cells and organisms. *Sci. Rep.* **8**, 15764. doi:10.1038/s41598-018-33592-8

Suzuki, K., Matsui, Y., Endo, K., Kubo, T., Hasegawa, T., Kimura, T., Ohtani, O. and Yasui, N. (2010). Myxoid liposarcoma with EWS-CHOP type 1 fusion gene. *Anticancer Res.* **30**, 4679-4683.

Suzuki, K., Matsui, Y., Hashimoto, N., Naka, N., Araki, N., Kimura, T., Yoshikawa, H. and Ueda, T. (2012). Variation in myxoid liposarcoma: clinicopathological examination of four cases with detectable TLS-CHOP or EWS-CHOP fusion transcripts whose histopathological diagnosis was other than myxoid liposarcoma. *Oncol. Lett.* **3**, 293-296. doi:10.3892/ol.2011.480

Tan, A. Y., Riley, T. R., Coady, T., Bussemaker, H. J. and Manley, J. L. (2012). TLS/FUS (translocated in liposarcoma/fused in sarcoma) regulates target gene transcription via single-stranded DNA response elements. *Proc. Natl. Acad. Sci. USA* **109**, 6030-6035. doi:10.1073/pnas.1203028109

Thandapani, P. (2019). Super-enhancers in cancer. *Pharmacol. Ther.* **199**, 129-138. doi:10.1016/j.pharmthera.2019.02.014

Thelin-Järnum, S., Lassen, C., Panagopoulos, I., Mandahl, N. and Åman, P. (1999). Identification of genes differentially expressed in TLS-CHOP carrying myxoid liposarcomas. *Int. J. Cancer* **83**, 30-33. doi:10.1002/(SICI)1097-0215(19990924)83:1<30::AID-IJC6>3.0.CO;2-4

Thelin-Järnum, S., Göransson, M., Burguete, A. S., Olofsson, A. and Åman, P. (2002). The myxoid liposarcoma specific TLS-CHOP fusion protein localizes to nuclear structures distinct from PML nuclear bodies. *Int. J. Cancer* **97**, 446-450. doi:10.1002/ijc.1632

Thompson, V. F., Victor, R. A., Morera, A. A., Moinpour, M., Liu, M. N., Kisiel, C. C., Pickrel, K., Springhower, C. E. and Schwartz, J. C. (2018). Transcription-dependent formation of nuclear granules containing FUS and RNA Pol II. *Biochemistry* **57**, 7021-7032. doi:10.1021/acs.biochem.8b01097

Ubeda, M., Wang, X. Z., Zinszner, H., Wu, I., Habener, J. F. and Ron, D. (1996). Stress-induced binding of the transcriptional factor CHOP to a novel DNA control element. *Mol. Cell. Biol.* **16**, 1479-1489. doi:10.1128/MCB.16.4.1479

Wang, J., Choi, J.-M., Holehouse, A. S., Lee, H. O., Zhang, X., Jahnel, M., Maharana, S., Lemaitre, R., Pozniakovsky, A., Drechsel, D. et al. (2018). A molecular grammar governing the driving forces for phase separation of prion-like RNA binding proteins. *Cell* **174**, 688-699.e16. doi:10.1016/j.cell.2018.06.006

Wang, C., Zhang, E., Wu, F., Sun, Y., Wu, Y., Tao, B., Ming, Y., Xu, Y., Mao, R. and Fan, Y. (2019). The C-terminal low-complexity domain involved in liquid-liquid phase separation is required for BRD4 function in vivo. *J. Mol. Cell Biol.* **11**, 807-809. doi:10.1093/jmcb/mjz037

Wei, M.-T., Chang, Y.-C., Shimobayashi, S. F., Shin, Y., Strom, A. R. and Brangwynne, C. P. (2020). Nucleated transcriptional condensates amplify gene expression. *Nat. Cell Biol.* **22**, 1187-1196. doi:10.1038/s41556-020-00578-6

Yang, L., Gal, J., Chen, J. and Zhu, H. (2014). Self-assembled FUS binds active chromatin and regulates gene transcription. *Proc. Natl. Acad. Sci. USA* **111**, 17809-17814. doi:10.1073/pnas.1414004111

Yang, Y., Liu, L., Naik, I., Braunstein, Z., Zhong, J. and Ren, B. (2017). Transcription factor C/EBP homologous protein in health and diseases. *Front. Immunol.* **8**, 1612. doi:10.3389/fimmu.2017.01612

Yu, J. S. E., Colborne, S., Hughes, C. S., Morin, G. B. and Nielsen, T. O. (2019). The FUS-DDIT3 Interactome in myxoid liposarcoma. *Neoplasia* **21**, 740-1750. doi:10.1016/j.neo.2019.05.004

Zinszner, H., Sok, J., Immanuel, D., Yin, Y. and Ron, D. (1997). TLS (FUS) binds RNA in vivo and engages in nucleo-cytoplasmic shuttling. *J. Cell Sci.* **110**, 1741-1750. doi:10.1242/jcs.110.15.1741

Zuo, L., Zhang, G., Massett, M., Cheng, J., Guo, Z., Wang, L., Gao, Y., Li, R., Huang, X., Li, P. et al. (2021). Loci-specific phase separation of FET fusion oncoproteins promotes gene transcription. *Nat. Commun.* **12**, 1491. doi:10.1038/s41467-021-21690-7

FUS-CHOP Fusions

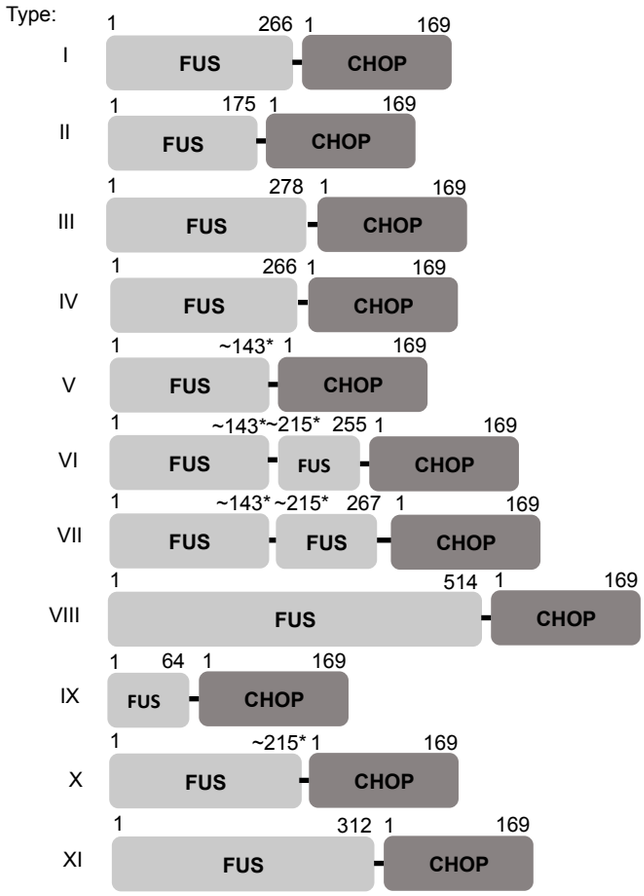

Fig. S1. Schematic of the 11 different types of FUS-CHOP fusions.
*Approximations based on reporting of FUS exon fusions/truncations but not precise codon sites.

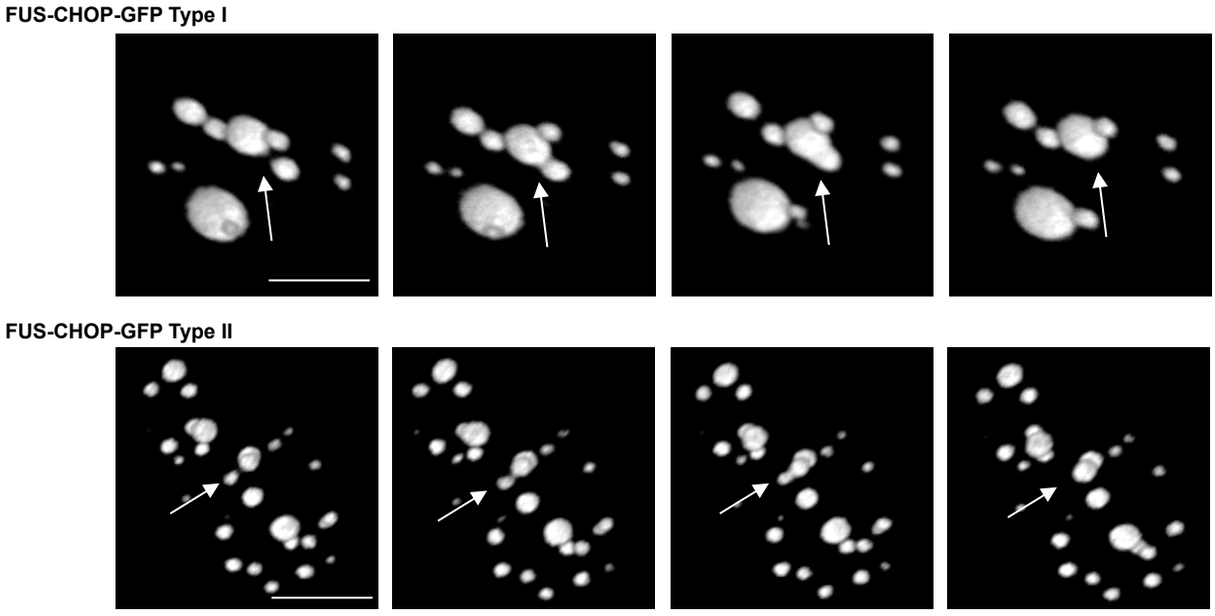

Fig. S2. Still frames from time course movies imaged by confocal microscopy of FUS-CHOP-eGFP type I and type II puncta fusing upon touching.

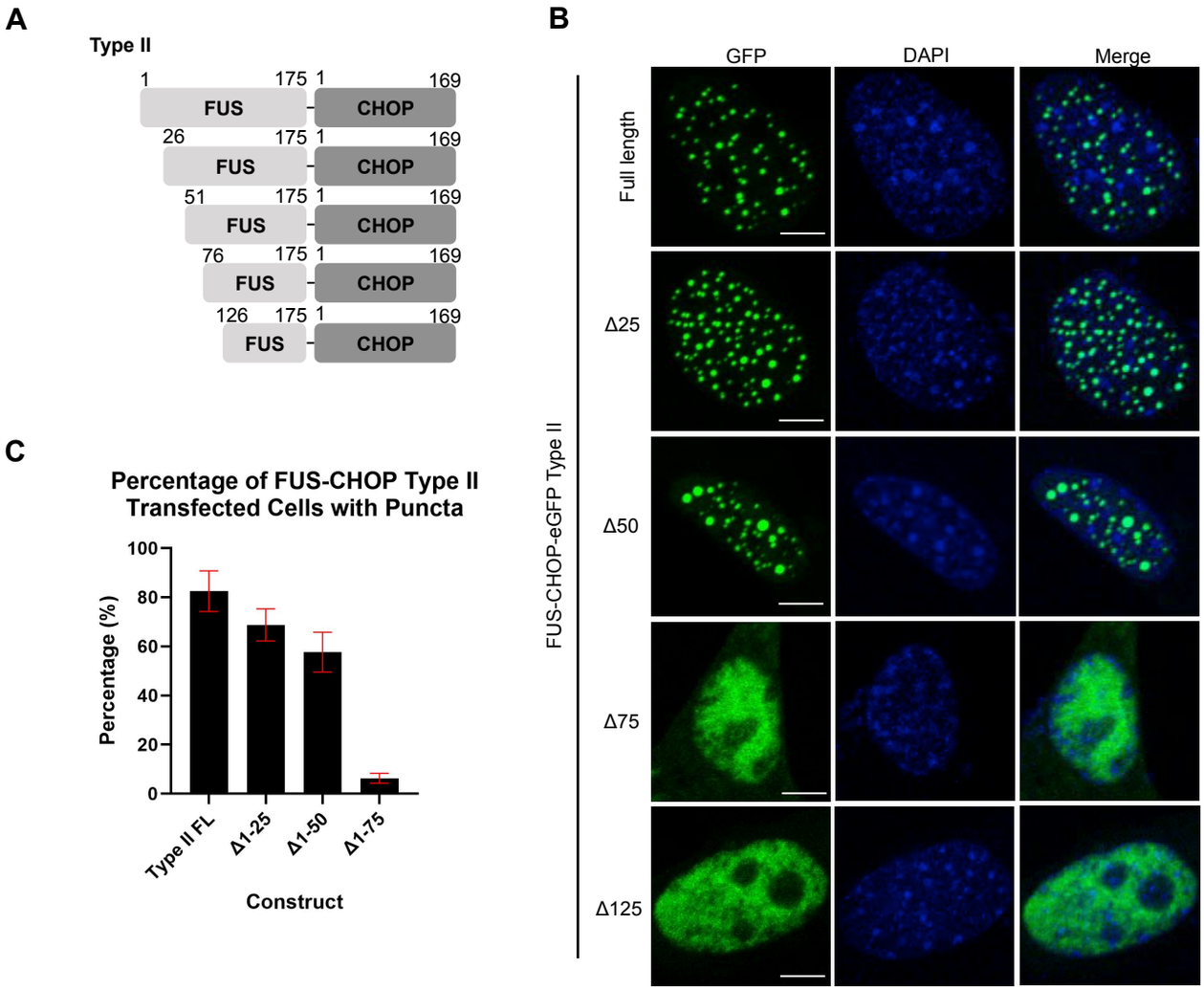

Fig. S3. A–Schematic of truncations made to FUS-CHOP-eGFP type II. B–Full-length or truncated FUS-CHOP-eGFP type II ectopically expressed in NIH 3T3 cells and imaged by confocal microscopy. Scale bar represents 5 µm. Representative data from three experimental replicates. C– Quantification of the percentage of transfected cells with nuclear puncta. Error bars represent the mean with 95% c.i. of measurements from three experimental replicates.

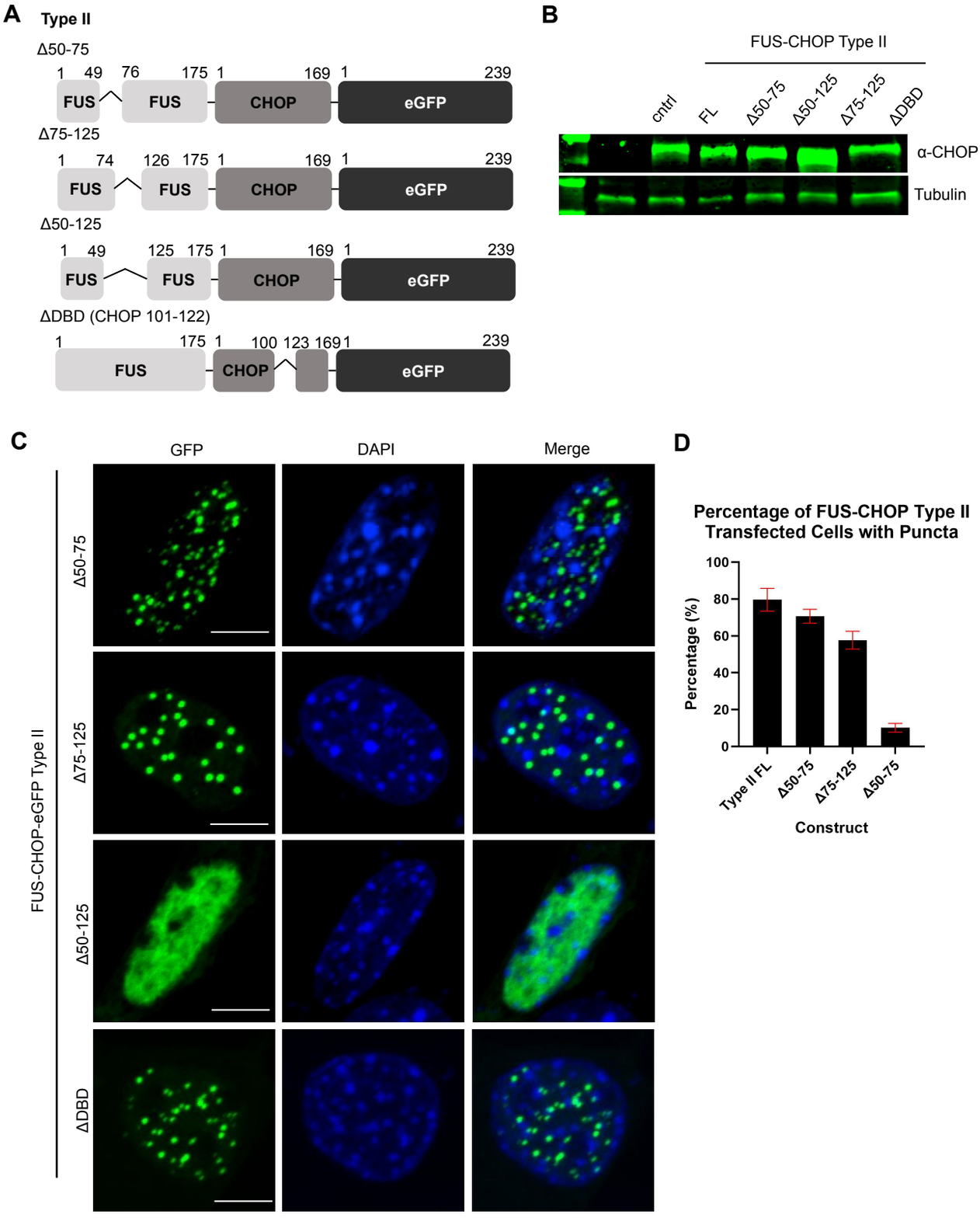

Fig. S4. A–Schematic of FUS-CHOP-eGFP type II internal truncations. B–NIH 3T3 cells transfected with full-length (FL) or truncated (Δ 50-75, Δ75-125, Δ50-125, or ΔDBD) FUS-CHOP-eGFP type II. Cell lysates were analyzed by Western Blot and probed with anti-CHOP and anti-tubulin antibodies. C– Confocal images of internally truncated FUS-CHOP-eGFP nuclear puncta type I or type II. Scale bar represents 5 μm. D- Percentage of transfected cells with nuclear puncta were quantified for each FUSCHOP-eGFP construct. Error bars represent the mean with 95% c.i. of measurements from three experimental replicates.

Table S1. Table denoting the number of tyrosine motifs removed in the FUS prion-like domain portion of FUS-CHOP truncations and internal deletions.

Construct	# of FUS PrLD tyrosine motifs removed
FUS-CHOP Δ25	3
FUS-CHOP Δ50	7
FUS-CHOP Δ75	11
FUS-CHOP Δ125	18
FUS-CHOP Δ50-75	5
FUS-CHOP Δ75-125	8
FUS-CHOP Δ50-125	11

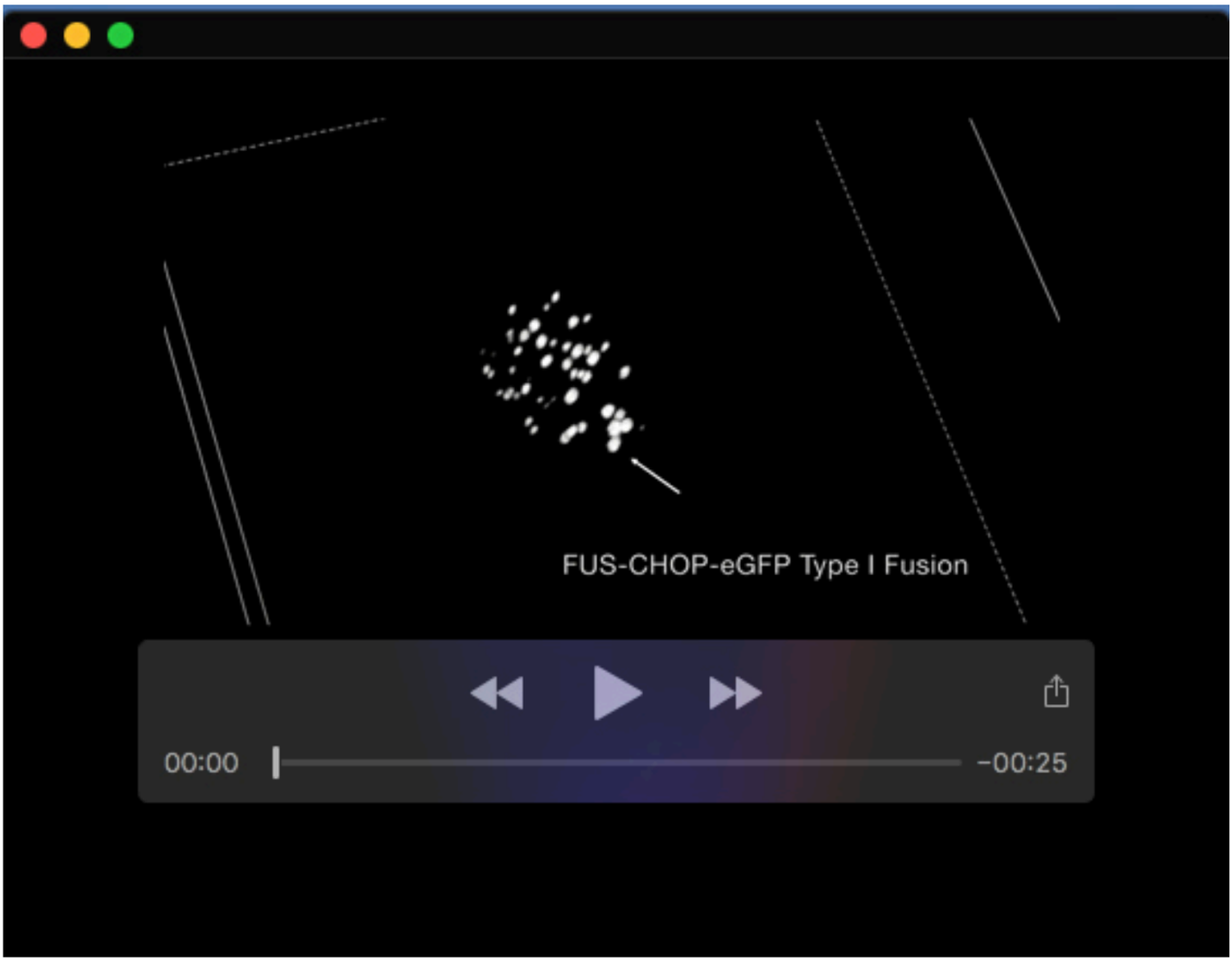

Movie 1. FUS-CHOP-eGFP puncta have liquid-like characteristics and undergo fusion in the nucleus.

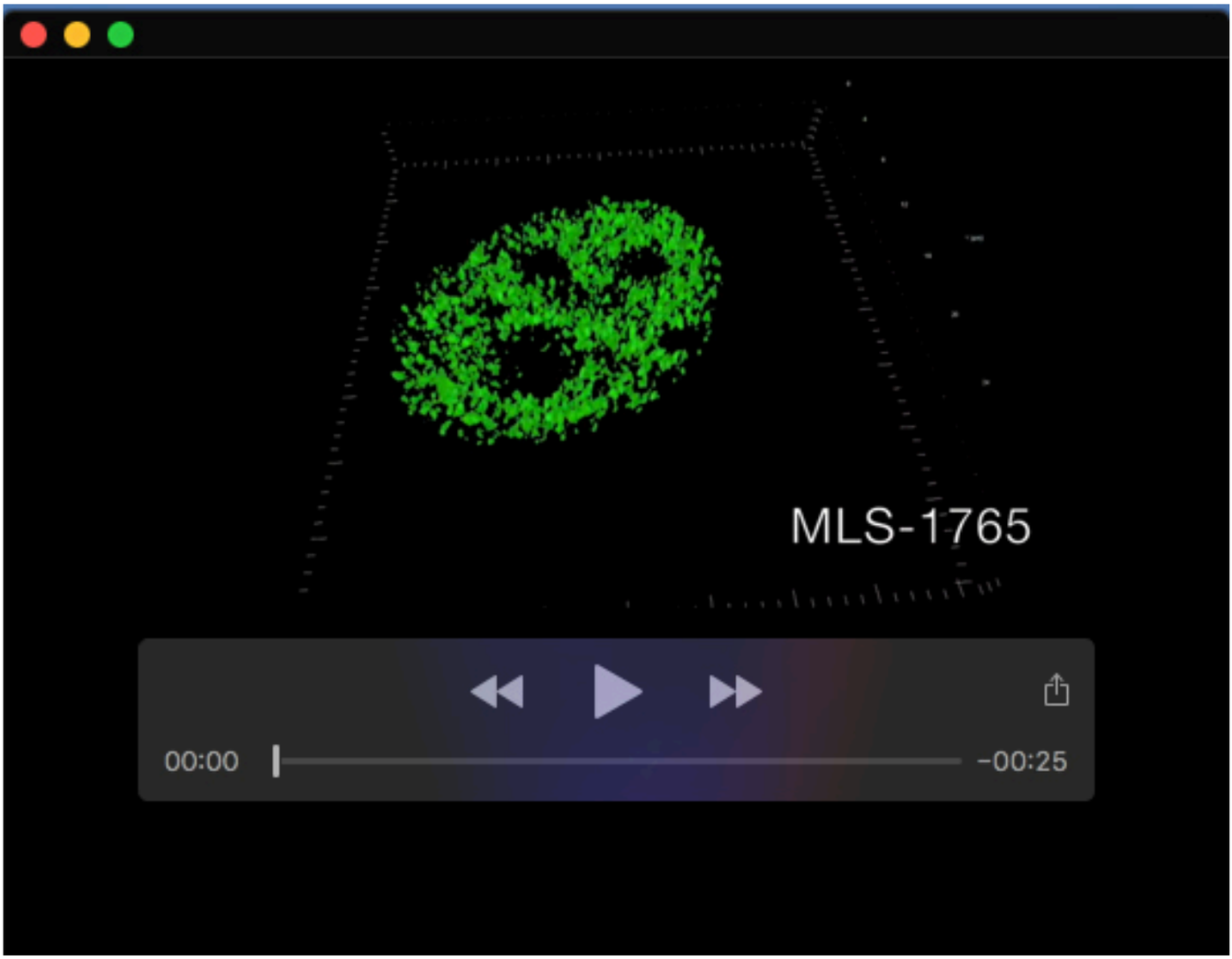

Movie 2. FUS-CHOP is localized to small nuclear puncta in Myxoid Liposarcoma cell lines.